medRxiv preprint doi: https://doi.org/10.1101/2021.07.13.21260404; this version posted January 21, 2022. The copyright holder for this preprint (which was not certified by peer review) is the author/funder, who has granted medRxiv a license to display the preprint in perpetuity.
All rights reserved. No reuse allowed without permission.

Pre-existing antibodies targeting a linear epitope on SARS-CoV-2 S2 cross-reacted with commensal gut bacteria and shaped vaccine induced immunity

Liqiu Jia[1, §], Shufeng Weng[2, §], Jing Wu[1, §], Xiangxiang Tian[3, 4], Yifan Zhang[3, 4], Xuyang Wang[1], Jing Wang[3, 5], Dongmei Yan[5], Wanhai Wang[4], Fang Fang[3], Zhaoqin Zhu[3, #], Chao Qiu[6, #], Wenhong Zhang[1, 2, 7, 8, #], Ying Xu[2, #], Yanmin Wan[1, 2, 9, #]

[1] Department of Infectious Diseases, National Medical Center for Infectious Diseases, Shanghai Key Laboratory of Infectious Diseases and Biosafety Emergency Response, Huashan Hospital, Shanghai Medical College, Fudan University, Shanghai, China;
[2] State Key Laboratory of Genetic Engineering, Institute of Genetics, School of Life Science, Fudan University, Shanghai, China;
[3] Shanghai Public Health Clinical Center, Fudan University, Shanghai, China;
[4] Clinical Laboratory, The First Affiliated Hospital of Zhengzhou University, Key Laboratory of Laboratory Medicine of Henan Province, Zhengzhou, Henan, P.R. China;
[5] Department of Immunology, School of Basic Medical, Jiamusi University, Jiamusi, Heilongjiang Province, China;
[6] Institutes of biomedical sciences & Shanghai Key Laboratory of Medical Epigenetics, Fudan University, Shanghai, China;
[7] National Clinical Research Center for Aging and Medicine, Huashan Hospital, Shanghai Medical College, Fudan University, Shanghai, China;
[8] Key Laboratory of Medical Molecular Virology (MOE/MOH) and Institutes of Biomedical Sciences, Shanghai Medical College, Fudan University, Shanghai, China.
[9] Department of radiology, Shanghai Public Health Clinical Center, Shanghai, China
[§] These authors contribute equally to this work.
[#] Correspondence should be addressed to: Zhaoqin Zhu, zhaoqinzhu@163.com; Chao Qiu, qiuchao@fudan.edu.cn; Wenhong Zhang, zhangwenhong@fudan.edu.cn; Ying Xu, yingxu2520@fudan.edu.cn; Yanmin Wan, yanmin_wan@fudan.edu.cn

Running title: SARS-CoV-2 antibody cross-reacts with gut bacteria

Word count: Abstract, 196; main text, 6810

NOTE: This preprint reports new research that has not been certified by peer review and should not be used to guide clinical practice.

medRxiv preprint doi: https://doi.org/10.1101/2021.07.13.21260404; this version posted January 21, 2022. The copyright holder for this preprint (which was not certified by peer review) is the author/funder, who has granted medRxiv a license to display the preprint in perpetuity. All rights reserved. No reuse allowed without permission.

Abstract

The origins of pre-existing SARS-CoV-2 cross-reactive antibodies and their potential impacts on vaccine efficacy have not been fully clarified. In this study, we demonstrated that S2 was the prevailing target of the pre-existing S protein cross-reactive antibodies in both healthy human and SPF mice. A dominant antibody epitope was identified on the connector domain of S2 (1147-SFKEELDKYFKNHT-1160, P144), which could be recognized by pre-existing antibodies in both human and mouse. Through metagenomic sequencing and fecal bacteria transplant, we proved that the generation of S2 cross-reactive antibodies was associated with commensal gut bacteria. Furthermore, six P144 specific monoclonal antibodies were isolated from naïve SPF mice and proved to cross-react with commensal gut bacteria collected from both human and mouse. Mice with high levels of pre-existing S2 cross-reactive antibodies mounted higher S protein specific binding antibodies, especially against S2, after being immunized with a SARS-CoV-2 S DNA vaccine. Similarly, we found that levels of pre-existing S2 and P144 reactive antibodies correlated positively with RBD specific binding antibody titers after two doses of inactivated SARS-CoV-2 vaccination in human. Finally, we provided data demonstrating that immunization of a SARS-CoV-2 S DNA vaccine could alter the gut microbiota compositions of mice.

Key words: Cross-reactive antibody, SARS-CoV-2, Spike protein, commensal gut bacteria, vaccine immunogenicity

medRxiv preprint doi: https://doi.org/10.1101/2021.07.13.21260404; this version posted January 21, 2022. The copyright holder for this preprint (which was not certified by peer review) is the author/funder, who has granted medRxiv a license to display the preprint in perpetuity. All rights reserved. No reuse allowed without permission.

Introduction

Antibodies are vital components of the immune system that mediate protection against infections (1). When confronting infections, the actual role of pre-existing antibody depends on the following features (2): High titers of broadly neutralizing antibodies can protect the host against infection. While, when the pre-existing antibodies are non-neutralizing or with only a narrow neutralizing spectrum, hosts may not be sterilely protected or only be protected against specific serotypes of viruses. In addition to defending hosts against infections, pre-existing antibodies can also impact host immune responses upon infection or vaccination (3-5), which is best exemplified by the observations showing that pre-existing antibodies shaped the recall immune responses against influenza (6, 7).

For most occasions, pre-existing antibodies in adults derive from previous infection or vaccination except some “naturally” produced, poly-reactive antibodies (2, 8). When encountering a newly emerged or mutated virus, cross-reactive antibodies induced by previously occurred, phylogenetically closely related viruses constitute the main body of the pre-existing cross-reactive antibodies. The effect of this kind of pre-existing antibodies has been extensively investigated especially for infections of influenza (3, 7, 9) and flaviviruses (10-12). Of note, previous infection by phylogenetically similar viruses is not the sole source of pre-existing cross-reactive antibodies, as it has been clearly clarified that pre-existing antibodies against HIV-1 gp41 may stem from exposures to certain commensal gut bacteria (13-15). Besides, autoimmune diseases caused by cross-reactivities between microbial and self-antigens also implied that commensal gut bacteria represent important sources of cross-reactive antibodies (16-19).

Pre-existing antibodies against SARS-CoV-2 have also been observed in uninfected healthy individuals, which are speculated to be engendered by previous exposures to human common cold coronaviruses (20-26) or SARS-CoV (27-29). Meanwhile, sequence analyses (30) and a clinical observation (31) suggest that pre-existing SARS-CoV-2 antibodies might be engendered by common human pathogens and childhood vaccination. Although these two explanations are not mutually exclusive, they both need more experimental evidence to support.

In this study, we found that higher levels of SARS-CoV-2 S2 protein specific

medRxiv preprint doi: https://doi.org/10.1101/2021.07.13.21260404; this version posted January 21, 2022. The copyright holder for this preprint (which was not certified by peer review) is the author/funder, who has granted medRxiv a license to display the preprint in perpetuity. All rights reserved. No reuse allowed without permission.

antibodies existed in both healthy human and naïve SPF mice. To track the potential origins of these pre-existing cross-reactive antibodies, we mapped and identified a dominant linear antibody epitope on S2, which could be recognized by pre-existing antibodies from both healthy human and naïve SPF mice. Monoclonal antibodies against this linear epitope were isolated from naïve SPF mice and proved to cross-react with commensal gut bacteria collected from both healthy human and naïve SPF mouse. Moreover, despite having been discussed iteratively (32, 33), the influences of pre-existing cross-reactive immunities on COVID-19 responses have not been clarified. Here we showed that high levels of pre-existing antibodies did not impair the immunogenicity of a candidate DNA vaccine encoding SARS-CoV-2 spike protein. On the contrary, mice with high levels of pre-existing antibodies mounted stronger S2 specific binding antibody responses compared with mice with low levels of pre-existing antibodies after immunization with a candidate DNA vaccine. Meanwhile, we showed that inoculation of the SARS-CoV-2 S DNA vaccine could significantly alter the gut microbiota compositions of mice.

Results

Pre-existing antibodies recognizing a dominant linear epitope on SARS-CoV-2 S2 protein were detected in both human and mice

Pre-existing antibodies cross-react with SARS-CoV-2 S protein have been found in uninfected individuals by multiple previous studies (22, 25, 26, 34). It was postulated that the pre-existing immunities against SARS-CoV-2 might be induced by previous exposure to seasonal human coronaviruses (22, 32, 33, 35, 36). However, contradictive evidence suggested that human common cold coronavirus infection did not necessarily induce antibodies cross-reactive with SARS-CoV-2 spike protein (28, 37, 38). In addition to this hypothesis, an alternative explanation suggested that the cross-reactive immunities to SARS-CoV-2 might derive from other common human pathogens and vaccines (30).

To track the origins of the pre-existing cross-reactive antibodies to SARS-CoV-2 spike protein, in this study, we first measured the levels of pre-existing S protein specific antibodies in healthy human individuals and SPF mice. Our data showed that the cross-reactive antibody responses against S2 were significantly stronger than those against S1 in plasma

medRxiv preprint doi: https://doi.org/10.1101/2021.07.13.21260404; this version posted January 21, 2022. The copyright holder for this preprint (which was not certified by peer review) is the author/funder, who has granted medRxiv a license to display the preprint in perpetuity. All rights reserved. No reuse allowed without permission.

samples of healthy human collected both pre (2016 cohort) and post (2020 cohort) the outbreak of COVID-19 pandemic (Figure 1A and 1B). More strikingly, our data showed that binding antibodies targeting S2 could also be detected in two strains of naïve SPF mice (Figure 1C and 1D). And this finding was further confirmed by Western-blotting (WB) assays, which showed that mouse sera with high OD values (Detected by ELISA) (Figure 2A) bound specifically with purified S2 while not S1 (Figure 2B). Quite interestingly, the WB results indicated that cross-reactive antibodies against S2 also existed in the serum of a mouse (#487) with no detectable ELISA binding signal (Figure 2A and 2B). We next performed linear antibody epitope mapping using an in-house developed method of peptide competition ELISA. Our data showed that a single peptide (P144, aa1145-aa1162, 18-mer) accounted for most of the observed pre-existing antibody responses towards S2 in mice (Supplementary Figure 1). Via employing a series of truncated peptides based on P144, we determined the minimal range of this epitope (1147-SFKEELDKYFKNHT-1160), which locates on the connector domain (adjacent to the N-terminal of HR2 domain) (Figure 2C). We also proved that antibodies recognizing this epitope widely existed in both healthy human and naïve SPF mice through competitive ELISA assays (Figure 3).

The P144 specific antibody responses could be engendered by exposures to certain commensal gut bacteria

To explore the potential origins of the pre-existed P144 specific antibodies, we first performed phylogenetic analyses among SARS-CoV-2 and other human coronaviruses. The results showed that the aa sequence of P144 was highly conserved among SARS-CoV-2 variants and SARS-CoV, while the similarities between P144 and MERS-CoV or seasonal human coronaviruses were relatively low, especially within the range of predicted antibody binding epitope (boxed fragment) (Supplementary Figure 2). The possibility of coronavirus infection in our SPF-mouse colonies was excluded by serum screenings using commercialized mouse hepatitis virus (MHV) antigen (Cat# SBJ-M0051-48T, SinBeiJia Biological Technology Co., Ltd, China) and antibody detection kits (Cat#SY-M02196, Shanghai Shuangying Biotechnology Co., Ltd, China) (Data not shown).

Subsequently, to investigate whether environmental factors contribute to the

medRxiv preprint doi: https://doi.org/10.1101/2021.07.13.21260404; this version posted January 21, 2022. The copyright holder for this preprint (which was not certified by peer review) is the author/funder, who has granted medRxiv a license to display the preprint in perpetuity. All rights reserved. No reuse allowed without permission.

induction of these S2 cross-reactive antibodies, we compared the levels of pre-existing S2 binding antibodies between mice housed in SPF condition and mice maintained in a sterile isolation pack. Our data showed that the levels of pre-existing S2 binding antibodies were significantly higher in SPF mice (Figure 4A). Through metagenomic sequencing, we further demonstrated that the compositions of commensal gut bacteria were significantly different between mice housed in different environments (Supplementary Figure 3A). The abundance of bacteroidaceae, prevotellaceace and parabacteroides increased significantly in the commensal gut bacteria of SPF mice (Figure 4B). Moreover, frequencies of memory B cells measured by B cell ELISPOT (Supplementary Figure 3B) and frequencies of S2 specific B cells (CD45+CD19+S2+) measured by flowcytometry (Supplementary Figure 3C) were significantly higher in mesenteric lymph nodes (MLNs) than those in spleens of mice with pre-existing S2 binding antibodies. Consistently, via 16s rDNA sequencing, we found that the gut microbiota compositions of SPF mice with different levels of pre-existing S2 binding antibodies might be different (Supplementary Figure 4). To further clarify the role of gut microbiota in the induction of S2 cross-reactive antibodies, mice fed in a sterile isolation pack were transplanted with fecal bacteria prepared from SPF mice (Figure 4C). We found that the abundances of P144 reactive antibodies in mouse sera significantly increased after fecal microbiota transplantation (FMT) (Figure 4D). These results collectively suggested that the S2 cross-reactive antibodies could be induced by exposures to certain microbial antigens.

P144 specific monoclonal antibodies reacted with commensal gut bacteria of both human and mouse and showed limited neutralizing activities

To probe the potential antigens that might induce the P144 binding antibodies, we isolated 6 mAbs from two naïve SPF mice (one C57BL/6J mouse and one BALB/c mouse) with high levels of pre-existing S2 specific antibody responses. The results of microscale thermophoresis (MST) assays showed that the binding affinities with S2 protein were similar among the 6 mAbs (F5, 2.07 μM; H9, 0.98 μM; E10, 3.53 μM; G13, 2.10 μM; M3,1.46 μM; G18, 2.25 μM) (Supplementary Figure 5). Five of these mAbs recognized P144 solely (Supplementary Figure 6A), while one mAb (clone M3) bound with P144 and

medRxiv preprint doi: https://doi.org/10.1101/2021.07.13.21260404; this version posted January 21, 2022. The copyright holder for this preprint (which was not certified by peer review) is the author/funder, who has granted medRxiv a license to display the preprint in perpetuity. All rights reserved. No reuse allowed without permission.

P103 simultaneously (Supplementary Figure 6B). Results of competitive ELISA showed that the minimal epitopes varied slightly among the five P144 specific mAbs, especially at the C-terminal of P144 (Supplementary Figure 6A). The neutralizing potentials of these isolated monoclonal antibodies were evaluated using a pseudo virus-based neutralization assay. Our results showed that these monoclonal antibodies exhibited limited neutralizing activity against 5 SARS-CoV-2 variants (Supplementary Figure 7), which might be partially explained by their relatively low affinities to S2 protein (Supplementary Figure 5).

To prove the cross-reactivities between S2 and commensal gut microbial antigens, whole cell lysates (WCL) of mouse and human commensal gut bacteria were prepared and used as antigens for WB assays, respectively. As shown in Figure 5A, specific bindings with the WCL of mixed fecal bacteria prepared from mice either with low levels of pre-existing antibodies (L) or with high levels of pre-existing antibodies (H) could be clearly visualized for each isolated mAbs. It was noteworthy that all mAbs except E10 strongly recognized a band around 180KD in the sample from mice with high pre-existing antibody responses. E10 predominantly recognized a band around 55KD in both samples, while stronger binding with the sample from mice with high pre-existing antibody responses could be visually observed (Figure 5A). Among the six mAbs, F5 showed the most diverse binding compacity. In addition to the band around 180KD, F5 bound with a band around 55KD (similar with E10) and a band between 40KD-55KD (Figure 5A). In comparison with the WB results of mouse samples, the recognized bands were less consistent across different human fecal bacteria samples (Figure 5B), presumably due to the individual to individual variation of gut microbiota composition. We found that a band around 70KD was recognized by most mAbs in 4 (lanes 1, 5, 6, 7) out of 7 samples and a band between 50KD-70KD was recognized by all mAbs in 3 (Lanes 2, 3, 7) out 7 samples. Our data showed that the recognition patterns towards each fecal bacteria sample were generally stable across different mAbs except E10 (Figure 5A and 5B). Then, we performed V(D)J gene sequencing for the 6 antibody clones. Our data showed that the same VH/VL gene combination (IGHV2-5*01, IGKV6-23*01) is used by 4 clones (F5, G18, H9 and M3) (Supplementary Table 1). Interestingly, among these 4 clones, F5 and M3 were isolated from a C57

medRxiv preprint doi: https://doi.org/10.1101/2021.07.13.21260404; this version posted January 21, 2022. The copyright holder for this preprint (which was not certified by peer review) is the author/funder, who has granted medRxiv a license to display the preprint in perpetuity. All rights reserved. No reuse allowed without permission.

mouse, while G18 and H9 were isolated from a BALB/c mouse, suggesting it might be a public antibody shared by different mice. G13 uses the same VH gene as the above 4 mAbs in combination with a different VL gene (IGLV2*02). The VH/VL gene usage (IGHV5-9*02, IGKV8-30*01) of E10 is completely different from other clones, which might explain its unique WB patterns shown in Figure 5A and 5B.

Proteins corresponding to specifically recognized bands were excised from Coomassie blue stained gels and analyzed by the mass spectrometry. For the mouse fecal bacteria samples, protein bands with molecular weights around 180KD, 100KD, 55KD-70KD and 40KD-55KD (indicated by arrows in Figure 5A, panel F5) were selected. For human fecal bacteria samples, protein bands with molecular weights around 50KD-70KD, 70KD and 70KD-100KD (indicated by arrows in Figure 5B, panel F5) were selected. The lists of proteins identified in mouse and human samples were shown in Table 2 and Table 3, respectively. Proteins with molecular weights corresponding approximately to the excised protein bands were identified for both human and mouse fecal bacteria samples. Of note, multiple proteins within the theoretical MW range of 58KD to 60KD were found to be identical between mouse and human samples, which included Fumarate hydratase class I (Accession# P14407), Formate-tetrahydrofolate ligase OS (Accession# Q189R2), Phosphoenolpyruvate carboxykinase (ATP) OS (Accession# C4ZBL1 and A6LFQ4) and 60 kDa chaperonin OS (Accession# A0Q2T1). To verify the cross-reactivity of the proteins detected by LC-MS, we selected *E. coli* (DH5α strain) as a representative target because *E. coli* derived Fumarate hydratase class I (Accession# P14407) were found in both human and mouse fecal bacteria samples. The result of WB assay showed that the P144 specific mAb (Clone F5) recognized multiple bands with MWs consistent with *E. coli* proteins identified by LC-MS (Figure 5C). Employing an in-house ELISA method, we further proved that one of the isolated mAbs (E10) bound specifically with purified microbial HSP60 and HSP70 proteins (Figure 5D and 5E), while it did not obviously bind with purified human HSP60 or HSP70 (Supplementary Figure 8).

Pre-existing S2 cross-reactive antibodies impacted specific immunities induced by a candidate COVID-19 DNA vaccine in mice

medRxiv preprint doi: https://doi.org/10.1101/2021.07.13.21260404; this version posted January 21, 2022. The copyright holder for this preprint (which was not certified by peer review) is the author/funder, who has granted medRxiv a license to display the preprint in perpetuity. All rights reserved. No reuse allowed without permission.

Pre-existing antibodies has been shown to be able to shape the recall immune responses upon influenza infection and vaccination (6). And the concern about how the pre-existing immunities may influence the effect of a SARS-CoV-2 vaccine has also attracted lots of attention (33). To investigate the impact of the pre-existing P144 antibodies on the immunogenicity of a candidate DNA vaccine, 18 BALB/c mice were divided into 3 groups according to their levels of pre-existing S2 binding antibodies and immunized with a DNA vaccine encoding the full length of SARS-CoV-2 S protein (Figure 6A and 6B). Our data showed that mice with high levels of pre-existing S2 binding antibodies mounted significantly higher S2 binding antibody responses after vaccination compared to mice with low or moderate levels of pre-existing S2 binding antibodies (Figure 6C). The average level of P144 specific antibody responses was also stronger in mice with high levels of pre-existing S2 binding antibodies than that of mice with low pre-existing S2 binding antibody responses (Figure 6D and 6E). By comparison, both the S1 binding antibody and the neutralizing antibody titers did not significantly differ among all groups, despite that mice with moderate or high levels of pre-existing antibodies tended to mount higher average titer of S1 binding antibodies (Figure 6F and 6G). Mice without vaccination showed neither obvious S1 binding antibody response nor neutralizing activity (Data not shown). We further investigated the influence of pre-existing antibodies on humoral immune responses in mouse respiratory tract after vaccination. And our data showed that the levels of S1 specific IgG in BALF were similar among the three groups after DNA vaccination (Figure 7A), while the average level of S2 specific IgG in BALF from mice with high pre-existing S2 binding antibodies was significantly higher than those from mice with low pre-existing antibodies (Figure 7B). S protein specific IgA response did not increase significantly after vaccination as compared with unvaccinated group (Figure 7C and 7D).

As the pre-existing antibodies in naïve SPF mice predominantly recognized P144 (Figure 2C and Supplementary Figure 1), we delineated the impact of pre-existing antibodies on the recognition of this epitope after vaccination. Our results showed that the minimum epitope recognition pattern by the sera of mice with high levels of pre-existing antibodies remained unchanged after vaccination (Figure 8). Whereas the minimum epitope recognized by the sera of mice with moderate and low levels of pre-existing antibodies altered at

medRxiv preprint doi: https://doi.org/10.1101/2021.07.13.21260404; this version posted January 21, 2022. The copyright holder for this preprint (which was not certified by peer review) is the author/funder, who has granted medRxiv a license to display the preprint in perpetuity. All rights reserved. No reuse allowed without permission.

either the N-terminal or both terminals of P144 (Figure 8).

In addition to antibody measurement, we compared S protein specific T cell responses among the three groups as well (Figure 9A). The results showed that the candidate DNA vaccine elicited robust S protein specific T cell responses in all groups (Figure 9). Although no statistical significance was reached, interesting trends were observed: First, mice with high levels of pre-existing S2 binding antibodies tended to mount relatively stronger S1 and S2 specific IFN-γ+ T cell responses (Figure 9B, 9C and 9D); second, as measured by the releases of IL-6, IL-2 and TNF-α, mice with high levels of pre-existing antibodies tended to mount stronger T cell responses against both S1 and S2 (Figure 9C and 9D). Mice without vaccination showed no S protein specific T cells responses (Data not shown). The major findings of this part of the study were validated by a repeated experiment (Supplementary Figure 9).

Pre-existing S2 cross-reactive antibodies correlated with RBD binding antibody responses after two-dose inactivated SARS-CoV-2 vaccination

To investigate how the pre-existing cross-reactive antibodies may influence the COVID-19 vaccine induced immunity, peripheral blood samples were collected from 28 healthy individuals who received two doses of an inactivated SARS-CoV-2 vaccine (Figure 10A). Correlation analyses showed that both the OD values (Figure 10B and 10C) and the titers (Supplementary Table 2) of pre-existing S2 reactive antibodies were significantly associated with RBD binding antibody titers at 14 days after immunization. Additionally, although not statistically significant, the pre-existing P144 binding antibody levels tended to correlate positively with neutralizing antibody responses after vaccination (P=0.0946) (Figure 10D).

Impact of SARS-CoV-2 S DNA vaccination on the compositions of mouse gut microbiota

To explore whether SARS-CoV-2 S DNA vaccination can affect the composition of gut bacteria, mouse stool samples were collected before and after vaccination and analyzed by 16s rDNA sequencing (Supplementary Figure 10A). The results showed that P144 specific antibody increased significantly after DNA vaccination (Supplementary Figure 10B). The PCA analysis showed that the bacterial genera composition of vaccinated mice

medRxiv preprint doi: https://doi.org/10.1101/2021.07.13.21260404; this version posted January 21, 2022. The copyright holder for this preprint (which was not certified by peer review) is the author/funder, who has granted medRxiv a license to display the preprint in perpetuity. All rights reserved. No reuse allowed without permission.

clearly clustered together (Supplementary Figure 10C). More specifically, at the genus level, abundances of candidatus saccharimonas and muribaculaceae increased significantly after DNA vaccination, while no significant increase was observed in PBS group (Supplementary Figure 10D).

Discussion

The origins of pre-existing cross-reactive immunities against SARS-CoV-2 have been investigated vigorously since the outbreak of the pandemic (39). Accumulating data suggest that cross-reactive T cells (33, 40-43) in SARS-CoV-2 unexposed human might be induced by previous infections of other hCoVs. While the origins of pre-existing cross-reactive antibodies could not be completely explained by previous infections of other coronaviruses, as recent studies revealed that the magnitude of antibody responses to SARS-CoV-2 S protein in the sera of patients with COVID-19 was not related to HCoVs' S titers (44) and immunization with coronaviruses OC43 did not induce significant SARS-CoV-2 S protein cross-reactive antibodies in mice. Moreover, it has also been observed that SARS-CoV-2 S protein specific binding antibody responses were weak in SARS-CoV-2 unexposed individuals with obvious binding antibody responses against S proteins of common cold hCoVs (45, 46).

To track the potential origins of the pre-existed cross-reactive antibodies targeting SARS-CoV-2 spike protein, in this study, we first screened the cross-reactive antibody responses in SARS-CoV-2 unexposed human plasma collected in 2020 and 2016, respectively. In both cohorts, we found that the magnitudes of S2 binding antibodies were significantly higher than those of S1 binding antibodies. This finding is consistent with previous studies showing that pre-existing S2 cross-reactive antibody responses are stronger than S1 cross-reactive antibody responses in SARS-CoV-2 unexposed individuals (26, 44, 47, 48). Since S2 cross-reactive antibody responses have also been observed in unexposed animals (44), we continued to screen the cross-reactive antibody responses in two strains of naïve SPF mice. Our data showed that the OD values of S2 cross-reactive antibodies were significantly higher than those of S1 cross-reactive antibodies in naïve BALB/c and C57BL/6 mice. Detections of mouse sera collected from another two independent SPF animal facilities confirmed this finding (Data not shown). We

medRxiv preprint doi: https://doi.org/10.1101/2021.07.13.21260404; this version posted January 21, 2022. The copyright holder for this preprint (which was not certified by peer review) is the author/funder, who has granted medRxiv a license to display the preprint in perpetuity. All rights reserved. No reuse allowed without permission.

also tried to detect the SARS-CoV-2 S protein specific T cells responses in mice with high pre-existing S2 cross-reactive antibodies using the IFN-γ ELISPOT assay, which showed that there was no pre-existing cross-reactive T cell response among these mice (Data not shown).

To facilitate the search of potential antigens that induced the cross-reactive antibodies, we identified a dominant antibody epitope (P144) through a method of competitive ELISA based linear antibody epitope mapping. P144 is located within the connector domain of S2 (aa1147-aa1160, directly N-terminal of the HR2 region). The same epitope has been predicted (30) and detected in both SARS-CoV-2 unexposed and infected individuals by multiple previous studies (22, 23, 25, 26, 32). In this study, we detected P144 specific antibody responses in plasma samples of healthy individuals collected in both 2020 and 2016. More interestingly, we found that the pre-existing S2 cross-reactive antibodies in naïve SPF mice were predominantly against this epitope. Of note, although the aa sequence of P144 is highly conserved among SARS-CoV-2 variants and SARS-CoV, its similarity with four seasonal hCoVs is relatively low. It has also been shown that this epitope was more frequently recognized than its homologous peptides from common cold hCoVs by antibodies of COVID-19 negative individuals (23). These evidence collectively implied that the pre-existing S2 specific antibodies might not be necessarily elicited by previous common cold coronavirus infections.

To unveil the origin of the pre-existing S2 binding antibodies in mice, we first measured S2 specific B cells by B cell ELISPOT and flowcytometry and found that the frequency of S2 specific B cells was significantly higher in mesenteric LN than in spleen, suggesting that the gastrointestinal tract might be the primary site where the cross-reactive B cells were activated. As gut bacteria can promote B cell diversification and stimulate antibody production in both T-dependent and -independent ways (49), we speculated that exposure to certain gut microbial antigens might account for the presence of the cross-reactive antibodies. To prove this hypothesis, we interrogated the relationship between the levels of pre-existing S2 reactive antibodies and the compositions of mouse gut microbiota. Our results showed that mice with different gut microbiota composition had different levels of pre-existing S2 cross-reactive antibodies, and vice versa (Supplementary Figure 4). Moreover, we found that transplantation of fecal bacteria isolated from SPF mice could

medRxiv preprint doi: https://doi.org/10.1101/2021.07.13.21260404; this version posted January 21, 2022. The copyright holder for this preprint (which was not certified by peer review) is the author/funder, who has granted medRxiv a license to display the preprint in perpetuity. All rights reserved. No reuse allowed without permission.

induce S2 reactive antibodies in mice bred in a sterile isolation pack. The above evidence suggested that the S2 reactive antibodies could be induced by exposure to certain commensal gut bacteria. Nonetheless, the gut microbiota might not be the only factor that can affect the generation of the cross-reactive antibodies, because we observed that mice housed in the same cage could harbor different levels of S2 reactive antibodies (Data not shown).

We are not able to define the bacterial strains contributing to the induction of P144 reactive antibodies in the current study, because it is technically hard to get pure cultures for each potential strain. Instead, we tried to identify potential microbial antigens that may induce the cross-reactive antibodies. To do so, we isolated six P144 specific monoclonal antibodies from a naïve BALB/c mouse and a naïve C57BL/6 mouse, respectively. All the six mAbs were confirmed to be able to bind with P144 and showed weak neutralizing compacities against five SARS-CoV-2 variants. Leveraging these mAbs, we detected the cross-reactive antigens in mouse and human fecal microbiota through WB assays. Compared with a control mouse IgG, specific bands were observed for each mAb, which proved the antibody cross-reactivities between SARS-CoV-2 and commensal gut bacteria. The strongly recognized protein bands were further analyzed by LC-MS. Our data showed that cross-reactive antigens derived from bacteroides and parabacteroides were frequently identified in fecal bacteria samples of both human and mouse, which was consistent with our metagenomic sequencing data showing that the abundance of bacteroides and parabacteroides was significantly higher in the commensal gut bacteria of mice with high pre-existing S2 binding antibody levels. More intriguingly, five cross-reactive microbial antigens were identified in mouse and human fecal samples simultaneously, implying that the S2 cross-reactive antibodies might naturally occur in different species of mammals.

According to our LC-MS results, few proteins of *E.coli* and HSP60/HSP70 proteins of multiple bacterial strains can be recognized by P144 reactive antibodies. These results were verified by experiments showing that P144 reactive mAbs could bind with the lysate of an E.coli strain (DH5α) and purified HSP60/HSP70 proteins. However, due to the limited availabilities of pure cultures of commensal gut bacteria and their protein derivatives, we were not able to verify all the potential reactive strains in this study. Alternatively, we tried to refine our LC-MS results through sequence similarity analysis. We

medRxiv preprint doi: https://doi.org/10.1101/2021.07.13.21260404; this version posted January 21, 2022. The copyright holder for this preprint (which was not certified by peer review) is the author/funder, who has granted medRxiv a license to display the preprint in perpetuity. All rights reserved. No reuse allowed without permission.

found that P144 shared varied identities with LC-MS captured proteins (40%-70%, length ≥ 8 aa residues) (Data not shown). The similarities are not high enough to support confident identifications of potential cross-reactive epitopes based on our current data. To clarify this issue, we plan to expand experimental screening through collaboration in future.

In parallel with tracking the initial antigens that induced the S2 cross-reactive antibodies, we investigated the impact of pre-existing antibodies on the immunogenicity of a candidate DNA vaccine as well. According to previous reports, pre-existing cross-reactive antibodies may influence the effects of different vaccines differentially (6, 50). In this study, we found that the pre-existing cross-reactive antibodies shaped the vaccine-induced immune responses in both mouse and human. Mice with high levels of pre-existing antibodies mounted stronger S2 binding antibodies in both peripheral blood and bronchial lavage after vaccination. More interestingly, we found that the pre-existing antibody levels correlated positively with post-vaccination RBD binding antibody titers in human. These findings proved that the pre-existing S2 binding antibodies could facilitate the generation of vaccine induced antibody responses. Through epitope mapping, we observed that the pre-existing antibodies strongly restricted the minimal epitope recognition in mice with high levels of pre-existing antibodies, which suggested that the imprint effect of pre-existing cross-reactive antibodies on vaccine induced antibody responses was primarily epitope specific. In addition to antibody response, we also found that the high levels of pre-existed S2 binding antibodies tended to improve specific T cell responses induced by SARS-CoV-2 S DNA vaccine. Since we did not perform the live virus challenge, it is still not clear how the pre-existing S2 cross-reactive antibodies will impact vaccine efficacy *in vivo*. Nonetheless, as both our results and a recently published study suggested that antibodies targeting P144 epitope could neutralize SARS-CoV-2 (51), we speculate that the pre-existing P144 cross-reactive antibodies may have protective effect. Besides, in this part of the study, we tried but found it may not be appropriate to test the influences of pre-existing antibodies on vaccine elicited immunities through passive antibody transfer, because: First, passive antibody transfer cannot generate S2 reactive memory B cells in recipient mice, which was observed in the mesenteric lymph nodes and spleens of mice with pre-existing S2 reactive

medRxiv preprint doi: https://doi.org/10.1101/2021.07.13.21260404; this version posted January 21, 2022. The copyright holder for this preprint (which was not certified by peer review) is the author/funder, who has granted medRxiv a license to display the preprint in perpetuity. All rights reserved. No reuse allowed without permission.

antibodies (Supplementary Figure 3). Second, we found that in vivo antibody level dropped dramatically within 48 hours after tail vein injection and it was technically difficult to maintain relatively stable in vivo antibody level for a long term.

A deep understanding of pre-existing cross-reactive antibodies against SARS-CoV-2 will enable better therapeutic, diagnostic and vaccine strategies. In this study, we provided evidence showing that antibodies targeting a conserved linear epitope on S2 cross-reacted with gut microbial antigens from both human and mouse, manifesting that some of the pre-existing cross-reactive antibodies might be induced by exposure to certain commensal gut bacteria. We proved that the pre-existing S2 cross-reactive antibodies did not impair the immunogenicity of a candidate DNA vaccine in a mouse model, while the SARS-CoV-2 S DNA vaccination could significantly change the composition of mouse gut microbiota. Further investigations into the functions of P144 cross-reactive antibodies may assist in delineating the role S2 specific antibody upon SARS-CoV-2 infection and elucidating the mechanisms underlying the gastrointestinal symptom caused by COVID-19 (52-54).

Materials and methods

Ethics statement

All experiments and methods were performed in accordance with relevant guidelines and regulations. Experiments using mice and samples of healthy human were approved by the Research Ethics Review Committee of the Shanghai Public Health Clinical Center Affiliated to Fudan University.

Plasma samples of healthy human

Two batches of plasma samples were collected from healthy individuals at the health screening clinic of Shanghai Public Health Clinical Center. A concurrent batch was collected in December 2020. All the 95 individuals enrolled in this batch reported no epidemiological link with confirmed COVID-19 patients and were confirmed to be free from any chronic or acute disease. Viral RNA tests confirmed that all individuals in this batch were free from SARS-CoV-2 infection. In addition, a historical batch of 78 plasma samples from healthy individual cohort (collected in 2016) were also measured for their cross reactivities with SARS-CoV-2 S protein. As the local prevalence in Shanghai

medRxiv preprint doi: https://doi.org/10.1101/2021.07.13.21260404; this version posted January 21, 2022. The copyright holder for this preprint (which was not certified by peer review) is the author/funder, who has granted medRxiv a license to display the preprint in perpetuity. All rights reserved. No reuse allowed without permission.

was extremely low during previous SARS-CoV-1 epidemic, we did not do the serum screening for previous SARS-CoV-1 infection. Instead, we collected the information regarding previous SARS-CoV-1 infection status through either questionnaire survey (for the 2020 cohort) or telephone follow-up (for the 2016 cohort). There is no self-reported previous SARS-CoV-1 infection among the two cohorts. Demographical information about these two cohorts was described in Table 1.

Detection of SARS-CoV-2 S1 and S2 specific binding antibodies

In-house enzyme-linked immunosorbent assays (ELISA) were developed to measure SARS-CoV-2 S1 and S2 specific binding antibodies. High-binding 96-well EIA plates (Cat# 9018, Corning, USA) were coated with purified SARS-CoV-2 S1 (Cat# 40591-V08H, Sino Biological, China), S2 proteins (Cat# 40590-V08B, Sino Biological, China), recombinant *E.coli* HSP60 (Cat#HSP-004, Prospec, Jsrael), *E.coli* HSP70 (Cat#HSP-006, Prospec, Jsrael), human HSP60 (Cat#HSP-016, Prospec, Jsrael) or human HSP70 (Cat#HSP-170, Prospec, Jsrael) at a final concentration of 1μg/ml in carbonate/bi-carbonate coating buffer (30mM $NaHCO_3$,10mM Na_2CO_3, pH 9.6). Subsequently, the plates were blocked with 1×PBS containing 5% milk for 1 hour at 37°C. Next, 100μl of diluted human plasma, mouse serum or mAbs was added to each well. After 1-hour incubation at 37°C, the plates were washed with 1×PBS containing 0.05% Tween20 for 5 times. Then, 100μl of a HRP labeled rabbit anti-human IgG antibody (Cat# ab6759, Abcam, UK) or goat anti-mouse IgG antibody (Cat# 115-035-003, Jackson Immuno Research, USA) diluted in 1×PBS containing 5% milk were added to each well and incubated for 1 hour at 37°C. After a second round of wash, 100μl of TMB substrate reagent (Cat# MG882, MESGEN, China) was added to each well. 15 minutes later, the color development was stopped by adding 100μl of 1M H_2SO_4 to each well and the values of optical density at $OD450_{nm}$ and $OD630_{nm}$ were measured using 800 TS microplate reader (Cat# 800TS, Biotek, USA).

Competitive ELISA

According to the reference sequence of SARS-CoV-2 (Genebank accession number: NC_045512), peptides (18-mer overlapping by 11 residues, purities >

medRxiv preprint doi: https://doi.org/10.1101/2021.07.13.21260404; this version posted January 21, 2022. The copyright holder for this preprint (which was not certified by peer review) is the author/funder, who has granted medRxiv a license to display the preprint in perpetuity. All rights reserved. No reuse allowed without permission.

95%) encompass the full length of S protein were synthesized by GL Biochem (Shanghai, China). The experiment procedure was generally similar with the afore mentioned in-house ELISA assays, except that the diluted mouse serum or human plasma were incubated with synthesized peptides (5μg/ml) or a non-relevant peptide ($OVA_{323-339}$) for 1 hour at room temperature before adding into the coated EIA plates.

FACS analysis of S2 specific B cells in mice

Spleen and mesenteric lymph nodes were isolated from naïve SPF mice and single-cell suspensions were freshly prepared. After counting, 1×10^6 single cells were resuspended in 100μl R10 (RPMI1640 containing 10% fatal bovine serum) and incubated with biotinylated S2 protein (Cat# 40590-V08B-B, Sino Biological, China) for 30 minutes at room temperature. After incubation, the cells were washed twice with 500μl R10. Then, the cells were incubated with the mixture of PE-anti-mouse CD19 (Cat# 152408, Biolegend, USA, 1μl/test), BV510-anti-mouse CD45 (Cat# 103137, Biolegend, USA, 1.25μl/test) and Streptavidin-IF647 (Cat# 46006, AAT Bioquest, USA, 0.2μl/test) at room temperature for 30 minutes. After washing, the stained cells were resuspended in 200μl 1×PBS and analyzed using a BD LSRFortessa™ Flow Cytometer. The data were analyzed using the FlowJo software (BD Biosciences, USA).

Preparation of P144 specific monoclonal antibodies

Monoclonal antibodies against P144 were prepared from one naïve BALB/c mouse and one naïve C57BL/6 mouse respectively using the hybridoma technique. Briefly, freshly isolated splenocytes were mixed and fused with SP2/0 cells at a ratio of 1:10. Hybridoma cell clones secreting P144 specific antibodies were screened by ELISA and monoclonal hybridoma cells were selected by multiple rounds of limited dilution. Selected clones of hybridoma cells were injected intraperitoneally into BALB/c×ICR hybrid mice. About 1-2 weeks later, peritoneal fluid was collected, and monoclonal IgG was purified using Protein A resin. The purities of monoclonal antibodies were verified using SDS-PAGE and the antibody concentrations were determined using a BCA kit (Cat# P0012, Beyotime Biotechnology, China).

medRxiv preprint doi: https://doi.org/10.1101/2021.07.13.21260404; this version posted January 21, 2022. The copyright holder for this preprint (which was not certified by peer review) is the author/funder, who has granted medRxiv a license to display the preprint in perpetuity. All rights reserved. No reuse allowed without permission.

588 **V(D)J gene sequencing of P144 reactive monoclonal antibodies**

589 The V(D)J genes of P144 reactive monoclonal antibodies were sequenced by
590 AZENTA life science. Briefly, total RNA was extracted from hybridoma cells
591 using Trizol reagent (Cat# R4801-02, Invitrogen, USA). 5` RACE was
592 performed with SMARTer RACE cDNA Amplification Kit (Cat# 634923,
593 Clontech, USA), total RNA input was 500-2000ng. V(D)J genes of heavy and
594 light chains were amplified by PCR. The PCR products were purified through
595 gel extraction using a QIAquick Gel Extraction Kit (Cat# 28704, Qiagen, USA).
596 NGS libraries were constructed by using VAHTS Universal DNA Library Prep
597 Kit for Illumina (Cat# ND607, Vazyme, China). The qualified libraries were
598 sequenced on the Illumina Miseq 2×300 platform (Illumina, San Diego, CA,
599 USA). Raw fastq files were first subject to quality assessment. Adapters and
600 bases with poor quality scores (Q value lower than 20) were removed using
601 Trimmomatic (v0.36) to generate clean data (trimmed data). Pandaseq (2.10)
602 was used to merge pair-end read. Merged sequences were processed by
603 IgBLAST software to identify the V(D)J sequences. The reference sequences
604 were obtained in IMGT database (IMGT, https://www.imgt.org/).
605
606 **Isolation of gut commensal bacteria and preparation of whole cell lysate**
607 **(WCL)**

608 About 2g of each fecal sample was suspended with 15ml sterile 1×PBS and
609 vortexed thoroughly to obtain uniform mixtures. After centrifugation at 200×g
610 for 5 min, the supernatants were collected, and the sediments were discarded.
611 This process was repeated twice. Next, all the supernatant samples were
612 centrifuged twice at 9000×g for 5 min and the supernatants were discarded.
613 The precipitated bacteria pellets were resuspended in 500μl of 1×PBS
614 (containing 1mM PMSF) and disrupted with an ultrasonic cell crusher (the
615 probe-type sonicator, Model JY92-II; Ningbo Scientz Biotechnology Co., Ltd,
616 China). After sonication, the samples were centrifuged at 10000rpm for 30
617 minutes to remove the cellular debris.
618
619 **Western blotting**
620 WCL containing 10μg of total protein was separated by SDS-PAGE (10%
621 acrylamide gels) and then transferred onto a PVDF membrane (Cat#

medRxiv preprint doi: https://doi.org/10.1101/2021.07.13.21260404; this version posted January 21, 2022. The copyright holder for this preprint (which was not certified by peer review) is the author/funder, who has granted medRxiv a license to display the preprint in perpetuity.
All rights reserved. No reuse allowed without permission.

IPVH00010, Millipore, USA) or stained with Coomassie brilliant blue. After blocking with 5% skim milk for 2h, the membrane was incubated with a P144 specific monoclonal antibody or a control mouse IgG at a concentration of 1 µg/ml. After washing, the membrane was incubated with HRP conjugated rabbit anti-human IgG antibody (Cat# ab6759, Abcam, UK) or HRP conjugated goat anti-mouse IgG antibody (Cat # 115-035-003,Jackson Immuno Research, USA) diluted 1:5000 in TBST (Tris-buffered saline, pH 8.0, 0.05% Tween 20) containing 5% skim milk. After wash, the bands were developed with an ultra-sensitive ECL substrate (Cat# K-12045-D10, Advansta, USA). The area corresponding to the specific WB bands were excised from the gel stained with Coomassie blue and analyzed using the mass spectrometry.

Mass spectrometry analysis

The FASP digestion was adapted for the following procedures in Microcon PL-10 filters (Cat#MRCPRT010, Merck, USA). After three-time buffer displacement with 8 M Urea (Cat#U111898, Aladdin, China) and 100 mM Tris-HCl, pH 8.5, proteins were reduced by 10 mM DTT (Cat#646563, Sigma Aldrich, USA) at 37 °C for 30 min and followed by alkylation with 30 mM iodoacetamide at 25°C for 45 min in dark. Digestion was carried out with trypsin (enzyme/protein as 1:50) (Cat#T9201, Sigma Aldrich, USA) at 37°C for 12 h after a wash with 20% ACN (Cat#34851, Sigma Aldrich, USA) and three-time buffer displacement with digestion buffer (30 mM Tris-HCl, pH 8.0). After digestion, the solution was filtrated out and the filter was washed twice with 15% ACN, and all filtrates were pooled and vacuum-dried to reach a final concentration to 1 mg/ml. LC-MS analysis was performed using a nanoflow EASYnLC 1200 system (Thermo Fisher Scientific, Odense, Denmark) coupled to an Orbitrap Fusion Lumos mass spectrometer (Thermo Fisher Scientific, Bremen, Germany). A one-column system was adopted for all analyses. Samples were analyzed on a home-made C18 analytical column (75 µm i.d. × 25 cm, ReproSil-Pur 120 C18-AQ, 1.9 µm (Dr. Maisch GmbH, Germany). The mobile phases consisted of Solution A (0.1% formic acid (Cat#695076, Sigma Aldrich, USA) and Solution B (0.1% formic acid in 80% ACN). The derivatized peptides were eluted using the following gradients: 2–5% B in 2 min, 5–35% B in 100 min, 35–44% B in 6 min, 44–100% B in 3 min, 100% B for 10 min, at a flow rate of 200 nl/min. Data-dependent analysis was employed in MS analysis:

medRxiv preprint doi: https://doi.org/10.1101/2021.07.13.21260404; this version posted January 21, 2022. The copyright holder for this preprint (which was not certified by peer review) is the author/funder, who has granted medRxiv a license to display the preprint in perpetuity. All rights reserved. No reuse allowed without permission.

The time between master scan was 3s, and fragmented in HCD mode, normalized collision energy was 30.

Construction and preparation of a candidate DNA vaccine encoding SARS-CoV-2 full length S protein

The full-length *s* gene sequence of the reference SARS-CoV-2 strain was optimized according to the preference of human codon usage and synthesized by GENEWIZ life science company (Suchow, China). The codon optimized spike gene was subcloned into a eukaryotic expression vector (pJW4303, kindly gifted by Dr. Shan Lu's Laboratory at the University of Massachusetts) (55, 56). And the sequence of inserted gene was verified by Sanger sequencing (Sangon Biotech Co., Ltd., Shanghai, China). An EndoFree Plasmid Purification Kit (Cat#12391, Qiagen, Hilden, USA) was used to prepare the recombinant plasmid for mouse vaccination.

Mouse vaccination

Peripheral blood samples were collected from female adult mice and pre-existing S2 binding antibodies were measured using the previously described in-house ELISA method. According to their pre-existing S2 binding antibody levels (at 1:100 dilution of serum), the mice were divided into three groups: low ($0.015 < OD_{450nm-630nm} \leq 0.130$, n=6), moderate ($0.130 < OD_{450nm-630nm} \leq 0.750$, n=6) and high ($OD_{450nm-630nm} > 0.750$, n=6). All mice were immunized intramuscularly with the candidate S protein DNA vaccine (50μg/mouse) for three times at an interval of 2 weeks. Three weeks post the third vaccination, the mice were euthanized. Peripheral blood, bronchial lavage and spleen were collected for assays of S protein specific immune responses.

Metagenomic and 16s rDNA sequencing of mouse gut microbiota

Metagenomic DNA and 16s rDNA were sequenced by SHANGHAI BIOCHIP CO., LTD. For metagenomic DNA sequencing, bacterial DNA was extracted from fecal samples using a TIANamp Stool DNA Kit (Cat#DP328, TIANGEN, China). Then, a total amount of 1μg DNA per sample was used as input material for the DNA sample preparations. Metagenomic sequencing libraries were generated using NEBNext® Ultra™ DNA Library Prep Kit for Illumina

medRxiv preprint doi: https://doi.org/10.1101/2021.07.13.21260404; this version posted January 21, 2022. The copyright holder for this preprint (which was not certified by peer review) is the author/funder, who has granted medRxiv a license to display the preprint in perpetuity. All rights reserved. No reuse allowed without permission.

(Cat#E7103, NEB, USA) following manufacturer's recommendations. Constructed libraries were analyzed for size distribution by Agilent 2100 Bioanalyzer and quantified using real-time PCR. The clustering of the index-coded samples was performed on a cBot Cluster Generation System. After cluster generation, the library preparations were sequenced on an Illumina Novaseq 6000 platform and paired-end reads were generated.

For 16s rDNA sequencing, fragments of 16s rDNA were amplified with specific barcoded primers 338F (5'-CCTAYGGGRBGCASCAG-3') and 806R (5'-GGACTACNNGGGTATCTAAT-3'). After purification of the PCR product, sequencing libraries were generated using NEBNext® Ultra™ DNA Library Prep Kit for Illumina (Cat#E7654, NEB, USA) following manufacturer's recommendations. After quality evaluation, the library was sequenced on an Illumina Novaseq 6000 platform and 250bp paired-end reads were generated.

SARS-CoV-2 pseudo-virus neutralization assay

VSV-backboned SARS-CoV-2 pseudo-viruses were prepared according to a reported method (57). The neutralization assay was conducted by following the previously described procedure (57, 58). Briefly, 100μl of serially diluted mice sera were added into 96-well cell culture plates. Then, 50μl of pseudo-viruses with a titer of 13000 $TCID_{50}$/ml were added into each well and the plates were incubated at 37°C for 1 hour. Next, Vero cells were added into each well (2×10^4 cells/well) and the plates were incubated at 37°C in a humidified incubator with 5% CO_2. 24 hours later, luminescence detection reagent (Bright-Glo™ Luciferase Assay System, Promega, USA) was added to each well following the manufacturer`s instruction. The luminescence was measured using a luminescence microplate reader (GloMax® Navigator Microplate Luminometer, Promega, USA) within 5 minutes. The Reed-Muench method was used to calculate the virus neutralization titer. Antibody neutralization titers were presented as 50% maximal inhibitory concentration (IC_{50}).

Detections of S protein specific cellular immune responses

SARS-CoV-2 S protein specific IFN-γ releases were measured using the method of enzyme-linked immunosorbent spot (ELISPOT) assays (Cat# 551083, BD Bioscience, USA) according to a previously described procedure

medRxiv preprint doi: https://doi.org/10.1101/2021.07.13.21260404; this version posted January 21, 2022. The copyright holder for this preprint (which was not certified by peer review) is the author/funder, who has granted medRxiv a license to display the preprint in perpetuity. All rights reserved. No reuse allowed without permission.

(59). Briefly, the 96-well ELISPOT plates were coated with purified anti-mouse IFN-γ monoclonal antibody overnight at 4°C. Then, the plates were blocked and 2×10^5 fresh splenocytes were added into each well and incubated with peptide pools for 20 hours at 37°C in a humidified incubator with 5% CO_2. The final concentration for each peptide was 1μg/ml. After incubation, detecting antibody and Avidin-HRP were added sequentially. Finally, the plates were developed using the BD™ ELISPOT AEC Substrate Set (Cat#551951, BD Bioscience, USA) according to the manufacturer's manual. Spots representing IFN-γ producing cells were enumerated using an automated ELISPOT plate reader (ChampSpot III Elispot Reader, Saizhi, Beijing, China). At the same time, the supernatants in the wells of ELISPOT plates were also collected for detecting secreted cytokines using a multiplexed cytokine beads array kit (Cat#741054, Biolegend, USA).

Statistical analysis

All statistical analyses were performed using GraphPad Prism 8 (GraphPad Software, Inc., La Jolla, CA, USA). Comparisons between two groups were conducted by the method of *t*-test. Comparisons among three or more group were done using one-way ANOVA. $P<0.05$ was considered as statistically significant.

Acknowledgements

We thank Miss Zhangyufan He from Huashan Hospital, Fudan University, for her kind help with the language polishing. This work was funded by the National Natural Science Foundation of China (Grant No. 81971559, 82041010, 81971900, 31872744), National Science and Technology Major Project (Grant No. 2018ZX10731301-004, 2018ZX10302302-002 and 2018ZX10301-404-002-003) and the Science and Technology Commission of Shanghai Municipality (Grant No. 20411950400).

Author contributions

Y.M.W., Y.X., C.Q., Z.Q.Z. and W.H.Z. designed the study. L.Q.J., S.F.W., Y.M.W., X.X.T., Y.F.Z., J.W., X.Y.W., and J.W. conducted the experiments.

medRxiv preprint doi: https://doi.org/10.1101/2021.07.13.21260404; this version posted January 21, 2022. The copyright holder for this preprint (which was not certified by peer review) is the author/funder, who has granted medRxiv a license to display the preprint in perpetuity.
All rights reserved. No reuse allowed without permission.

Y.M.W., L.Q.J. and S.F.W. analyzed the data and drafted the manuscript. Y.M.W., Y.X., C.Q., Z.Q.Z., W.H.Z. and F.F. revised the manuscript. D.M.Y. and W.H.W. provided intellectual inputs in tackling technical challenges in tracking the potential cross-reacting antigens.

Conflict of Interest

The authors declare that they have no relevant conflicts of interest.

Data availability

The data of metagenomic analysis of gut microbiota has been deposited to the NCBI Sequence Read Archive (SRA) database with the accession number PRJNA747837.

References

1. Lu LL, Suscovich TJ, Fortune SM, Alter G. Beyond binding: antibody effector functions in infectious diseases. Nature reviews Immunology. 2018;18(1):46-61.
2. Warter L, Appanna R, Fink K. Human poly- and cross-reactive anti-viral antibodies and their impact on protection and pathology. Immunologic research. 2012;53(1-3):148-61.
3. Cobey S, Hensley SE. Immune history and influenza virus susceptibility. Current opinion in virology. 2017;22:105-11.
4. Mok DZL, Chan KR. The Effects of Pre-Existing Antibodies on Live-Attenuated Viral Vaccines. Viruses. 2020;12(5).
5. Zimmermann P, Curtis N. Factors That Influence the Immune Response to Vaccination. Clinical microbiology reviews. 2019;32(2).
6. Dugan HL, Guthmiller JJ, Arevalo P, Huang M, Chen YQ, Neu KE, et al. Preexisting immunity shapes distinct antibody landscapes after influenza virus infection and vaccination in humans. Science translational medicine. 2020;12(573).
7. Zhang A, Stacey HD, Mullarkey CE, Miller MS. Original Antigenic Sin: How First Exposure Shapes Lifelong Anti-Influenza Virus Immune Responses. Journal of immunology (Baltimore, Md : 1950). 2019;202(2):335-40.
8. Boes M. Role of natural and immune IgM antibodies in immune responses. Molecular immunology. 2000;37(18):1141-9.
9. Auladell M, Jia X, Hensen L, Chua B, Fox A, Nguyen THO, et al. Recalling the Future: Immunological Memory Toward Unpredictable Influenza Viruses. Frontiers in immunology. 2019;10:1400.
10. St. John AL, Rathore APS. Adaptive immune responses to primary and secondary dengue virus infections. Nature Reviews Immunology. 2019;19(4):218-30.
11. Izmirly AM, Alturki SO, Alturki SO, Connors J, Haddad EK. Challenges in Dengue Vaccines Development: Pre-existing Infections and Cross-Reactivity. 2020;11(1055).
12. Andrade P, Gimblet-Ochieng C, Modirian F, Collins M, Cárdenas M, Katzelnick LC, et al. Impact

medRxiv preprint doi: https://doi.org/10.1101/2021.07.13.21260404; this version posted January 21, 2022. The copyright holder for this preprint (which was not certified by peer review) is the author/funder, who has granted medRxiv a license to display the preprint in perpetuity. All rights reserved. No reuse allowed without permission.

of pre-existing dengue immunity on human antibody and memory B cell responses to Zika. Nature Communications. 2019;10(1):938.

13. Liao HX, Chen X, Munshaw S, Zhang R, Marshall DJ, Vandergrift N, et al. Initial antibodies binding to HIV-1 gp41 in acutely infected subjects are polyreactive and highly mutated. The Journal of experimental medicine. 2011;208(11):2237-49.

14. Bonsignori M, Liao HX, Gao F, Williams WB, Alam SM, Montefiori DC, et al. Antibody-virus co-evolution in HIV infection: paths for HIV vaccine development. Immunological reviews. 2017;275(1):145-60.

15. Williams WB, Liao HX, Moody MA, Kepler TB, Alam SM, Gao F, et al. HIV-1 VACCINES. Diversion of HIV-1 vaccine-induced immunity by gp41-microbiota cross-reactive antibodies. Science (New York, NY). 2015;349(6249):aab1253.

16. Zitvogel L, Ayyoub M, Routy B, Kroemer G. Microbiome and Anticancer Immunosurveillance. Cell. 2016;165(2):276-87.

17. Leng Q, Tarbe M, Long Q, Wang F. Pre-existing heterologous T-cell immunity and neoantigen immunogenicity. Clinical & translational immunology. 2020;9(3):e01111.

18. Sioud M. T-cell cross-reactivity may explain the large variation in how cancer patients respond to checkpoint inhibitors. Scandinavian journal of immunology. 2018;87(3).

19. Rose NR. Negative selection, epitope mimicry and autoimmunity. Current opinion in immunology. 2017;49:51-5.

20. Anderson EM, Goodwin EC, Verma A, Arevalo CP, Bolton MJ, Weirick ME, et al. Seasonal human coronavirus antibodies are boosted upon SARS-CoV-2 infection but not associated with protection. Cell. 2021.

21. Galipeau Y, Greig M, Liu G, Driedger M, Langlois MA. Humoral Responses and Serological Assays in SARS-CoV-2 Infections. Frontiers in immunology. 2020;11:610688.

22. Klompus S, Leviatan S, Vogl T, Kalka IN, Godneva A, Shinar E, et al. Cross-reactive antibody responses against SARS-CoV-2 and seasonal common cold coronaviruses. 2020:2020.09.01.20182220.

23. Shrock E, Fujimura E, Kula T, Timms RT, Lee IH, Leng Y, et al. Viral epitope profiling of COVID-19 patients reveals cross-reactivity and correlates of severity. Science (New York, NY). 2020;370(6520).

24. Ortega N, Ribes M, Vidal M, Rubio R, Aguilar R, Williams S, et al. Seven-month kinetics of SARS-CoV-2 antibodies and protective role of pre-existing antibodies to seasonal human coronaviruses on COVID-19. 2021:2021.02.22.21252150.

25. Ladner JT, Henson SN, Boyle AS, Engelbrektson AL, Fink ZW, Rahee F, et al. Epitope-resolved profiling of the SARS-CoV-2 antibody response identifies cross-reactivity with endemic human coronaviruses. Cell reports Medicine. 2021;2(1):100189.

26. Ng KW, Faulkner N, Cornish GH, Rosa A, Harvey R, Hussain S, et al. Preexisting and de novo humoral immunity to SARS-CoV-2 in humans. Science (New York, NY). 2020;370(6522):1339-43.

27. Yang R, Lan J, Huang B, A R, Lu M, Wang W, et al. Lack of antibody-mediated cross-protection between SARS-CoV-2 and SARS-CoV infections. EBioMedicine. 2020;58:102890.

28. Lv H, Wu NC, Tsang OT, Yuan M, Perera R, Leung WS, et al. Cross-reactive Antibody Response between SARS-CoV-2 and SARS-CoV Infections. Cell reports. 2020;31(9):107725.

29. Zhu Y, Yu D, Han Y, Yan H, Chong H, Ren L, et al. Cross-reactive neutralization of SARS-CoV-2 by serum antibodies from recovered SARS patients and immunized animals. Science advances. 2020;6(45).

medRxiv preprint doi: https://doi.org/10.1101/2021.07.13.21260404; this version posted January 21, 2022. The copyright holder for this preprint (which was not certified by peer review) is the author/funder, who has granted medRxiv a license to display the preprint in perpetuity.
All rights reserved. No reuse allowed without permission.

30. Reche PA. Potential Cross-Reactive Immunity to SARS-CoV-2 From Common Human Pathogens and Vaccines. Frontiers in immunology. 2020;11:586984.
31. Sumbul B, Sumbul HE, Okyay RA, Gülümsek E, Şahin AR, Boral B, et al. Is there a link between pre-existing antibodies acquired due to childhood vaccinations or past infections and COVID-19? A case control study. PeerJ. 2021;9:e10910.
32. Majdoubi A, Michalski C, O'Connell SE, Dada S, Narpala SR, Gelinas JP, et al. A majority of uninfected adults show pre-existing antibody reactivity against SARS-CoV-2. JCI insight. 2021.
33. Sette A, Crotty S. Pre-existing immunity to SARS-CoV-2: the knowns and unknowns. Nature reviews Immunology. 2020;20(8):457-8.
34. Tso FY, Lidenge SJ, Peña PB, Clegg AA, Ngowi JR, Mwaiselage J, et al. High prevalence of pre-existing serological cross-reactivity against severe acute respiratory syndrome coronavirus-2 (SARS-CoV-2) in sub-Saharan Africa. International journal of infectious diseases : IJID : official publication of the International Society for Infectious Diseases. 2021;102:577-83.
35. Lipsitch M, Grad YH, Sette A, Crotty S. Cross-reactive memory T cells and herd immunity to SARS-CoV-2. Nature reviews Immunology. 2020;20(11):709-13.
36. Lee CH, Pinho MP, Buckley PR, Woodhouse IB, Ogg G, Simmons A, et al. Potential CD8+ T Cell Cross-Reactivity Against SARS-CoV-2 Conferred by Other Coronavirus Strains. Frontiers in immunology. 2020;11:579480.
37. Freeman B, Lester S, Mills L, Rasheed MAU, Moye S, Abiona O, et al. Validation of a SARS-CoV-2 spike protein ELISA for use in contact investigations and sero-surveillance. 2020:2020.04.24.057323.
38. Post N, Eddy D, Huntley C, van Schalkwyk MCI, Shrotri M, Leeman D, et al. Antibody response to SARS-CoV-2 infection in humans: A systematic review. PloS one. 2020;15(12):e0244126.
39. Doshi P. Covid-19: Do many people have pre-existing immunity? 2020;370:m3563.
40. Steiner S, Sotzny F, Bauer S, Na I-K, Schmueck-Henneresse M, Corman VM, et al. HCoV- and SARS-CoV-2 Cross-Reactive T Cells in CVID Patients. 2020;11(3347).
41. Mateus J, Grifoni A, Tarke A, Sidney J, Ramirez SI, Dan JM, et al. Selective and cross-reactive SARS-CoV-2 T cell epitopes in unexposed humans. 2020;370(6512):89-94.
42. Grifoni A, Weiskopf D, Ramirez SI, Mateus J, Dan JM, Moderbacher CR, et al. Targets of T Cell Responses to SARS-CoV-2 Coronavirus in Humans with COVID-19 Disease and Unexposed Individuals. Cell. 2020;181(7):1489-501.e15.
43. Braun J, Loyal L, Frentsch M, Wendisch D, Georg P, Kurth F, et al. SARS-CoV-2-reactive T cells in healthy donors and patients with COVID-19. Nature. 2020;587(7833):270-4.
44. Kim H, Seiler P, Jones JC, Ridout G, Camp KP, Fabrizio TP, et al. Antibody Responses to SARS-CoV-2 Antigens in Humans and Animals. Vaccines. 2020;8(4).
45. Anderson EM, Goodwin EC, Verma A, Arevalo CP, Bolton MJ, Weirick ME, et al. Seasonal human coronavirus antibodies are boosted upon SARS-CoV-2 infection but not associated with protection. Cell. 2021;184(7):1858-64.e10.
46. Song G, He W-t, Callaghan S, Anzanello F, Huang D, Ricketts J, et al. Cross-reactive serum and memory B-cell responses to spike protein in SARS-CoV-2 and endemic coronavirus infection. Nature Communications. 2021;12(1):2938.
47. Fraley E, LeMaster C, Banerjee D, Khanal S, Selvarangan R, Bradley T. Cross-reactive antibody immunity against SARS-CoV-2 in children and adults. Cellular & molecular immunology. 2021:1-3.
48. Nguyen-Contant P, Embong AK, Kanagaiah P, Chaves FA, Yang H, Branche AR, et al. S

medRxiv preprint doi: https://doi.org/10.1101/2021.07.13.21260404; this version posted January 21, 2022. The copyright holder for this preprint (which was not certified by peer review) is the author/funder, who has granted medRxiv a license to display the preprint in perpetuity. All rights reserved. No reuse allowed without permission.

887 Protein-Reactive IgG and Memory B Cell Production after Human SARS-CoV-2 Infection Includes
888 Broad Reactivity to the S2 Subunit. mBio. 2020;11(5).
889 49. Zhao Q, Elson CO. Adaptive immune education by gut microbiota antigens. Immunology.
890 2018;154(1):28-37.
891 50. Bradt V, Malafa S, von Braun A, Jarmer J, Tsouchnikas G, Medits I, et al. Pre-existing yellow
892 fever immunity impairs and modulates the antibody response to tick-borne encephalitis vaccination.
893 NPJ vaccines. 2019;4:38.
894 51. Pinto D, Sauer MM, Czudnochowski N, Low JS, Tortorici MA, Housley MP, et al. Broad
895 betacoronavirus neutralization by a stem helix-specific human antibody. Science (New York, NY).
896 2021.
897 52. Lee IC, Huo TI, Huang YH. Gastrointestinal and liver manifestations in patients with COVID-19.
898 Journal of the Chinese Medical Association : JCMA. 2020;83(6):521-3.
899 53. Jin X, Lian JS, Hu JH, Gao J, Zheng L, Zhang YM, et al. Epidemiological, clinical and virological
900 characteristics of 74 cases of coronavirus-infected disease 2019 (COVID-19) with gastrointestinal
901 symptoms. Gut. 2020;69(6):1002-9.
902 54. Mao R, Qiu Y, He JS, Tan JY, Li XH, Liang J, et al. Manifestations and prognosis of
903 gastrointestinal and liver involvement in patients with COVID-19: a systematic review and
904 meta-analysis. The lancet Gastroenterology & hepatology. 2020;5(7):667-78.
905 55. Lu S, Manning S, Arthos J. Antigen engineering in DNA immunization. Methods in molecular
906 medicine. 2000;29:355-74.
907 56. Fan W, Wan Y, Li Q. Interleukin-21 enhances the antibody avidity elicited by DNA prime and
908 MVA boost vaccine. Cytokine. 2020;125:154814.
909 57. Nie J, Li Q, Wu J, Zhao C, Hao H, Liu H, et al. Establishment and validation of a pseudovirus
910 neutralization assay for SARS-CoV-2. Emerging microbes & infections. 2020;9(1):680-6.
911 58. Li Q, Wu J, Nie J, Zhang L, Hao H, Liu S, et al. The Impact of Mutations in SARS-CoV-2 Spike
912 on Viral Infectivity and Antigenicity. Cell. 2020;182(5):1284-94.e9.
913 59. Ren Y, Wang N, Hu W, Zhang X, Xu J, Wan Y. Successive site translocating inoculation
914 potentiates DNA/recombinant vaccinia vaccination. Scientific reports. 2015;5:18099.

(which was not certified by peer review) is the author/funder, who has granted medRxiv a license to display the preprint in perpetuity.
All rights reserved. No reuse allowed without permission.

Figures and Figure legends

Figure 1

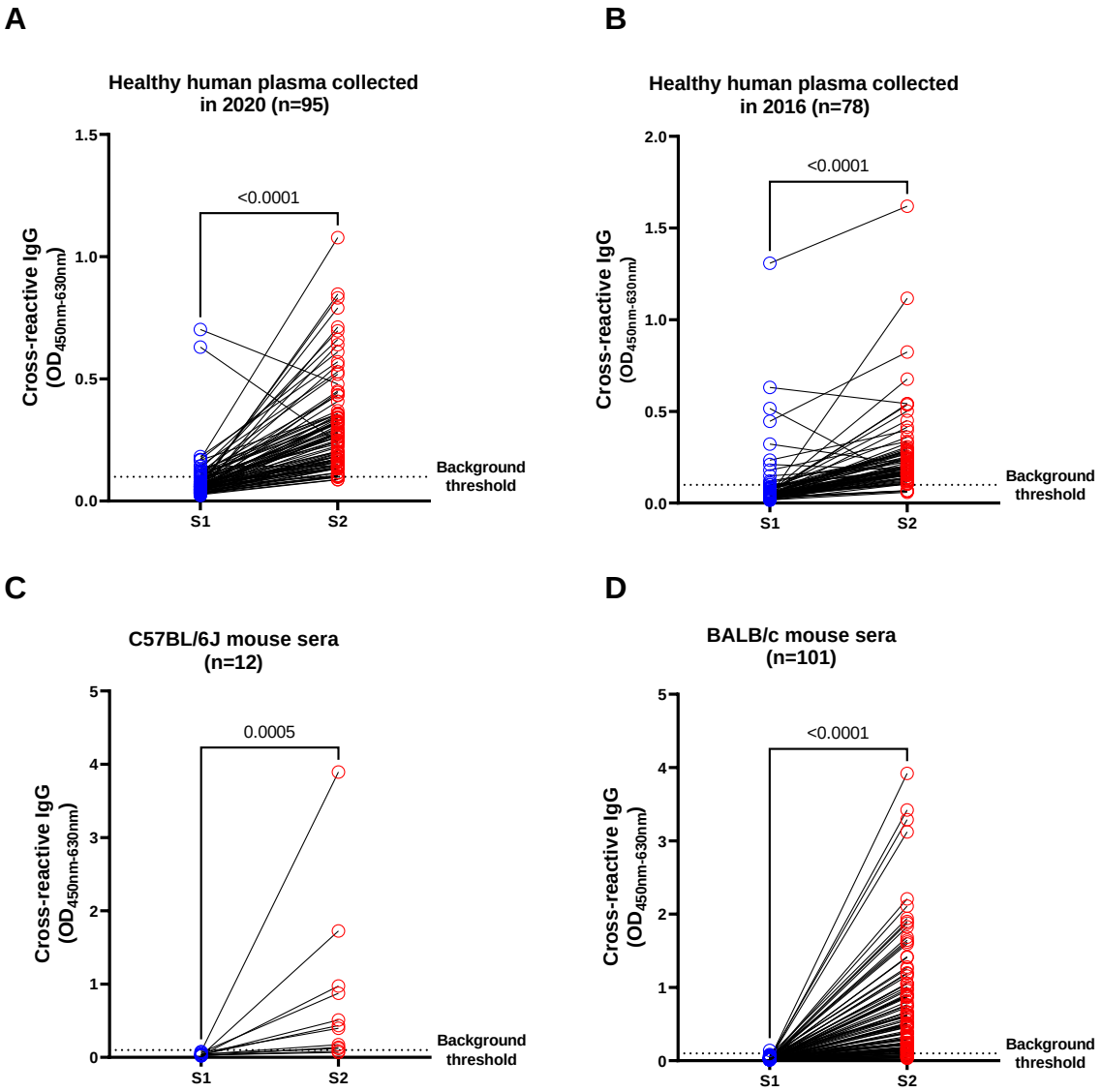

Figure 1 Pre-existing cross-reactive antibodies against SARS-CoV-2 S protein observed in both healthy human and naïve SPF mice predominantly targeted S2. The pre-existing cross-reactive antibodies against S1 and S2 were measured using an in-house ELISA method (Sample dilution factor: 100). (**A**) Plasma samples of healthy individuals collected in 2020 (n=95). (**B**) Plasma samples of healthy individuals collected in 2016 (n=78). (**C**) Sera of naïve C57BL/6J mice (n=12). (**D**) Sera of naïve BALB/c mice (n=101). The dotted lines show the threshold of background (3 folds of the average background OD). Statistical analyses were performed using the method of paired t-test.

(which was not certified by peer review) is the author/funder, who has granted medRxiv a license to display the preprint in perpetuity.
All rights reserved. No reuse allowed without permission.

Figure 2

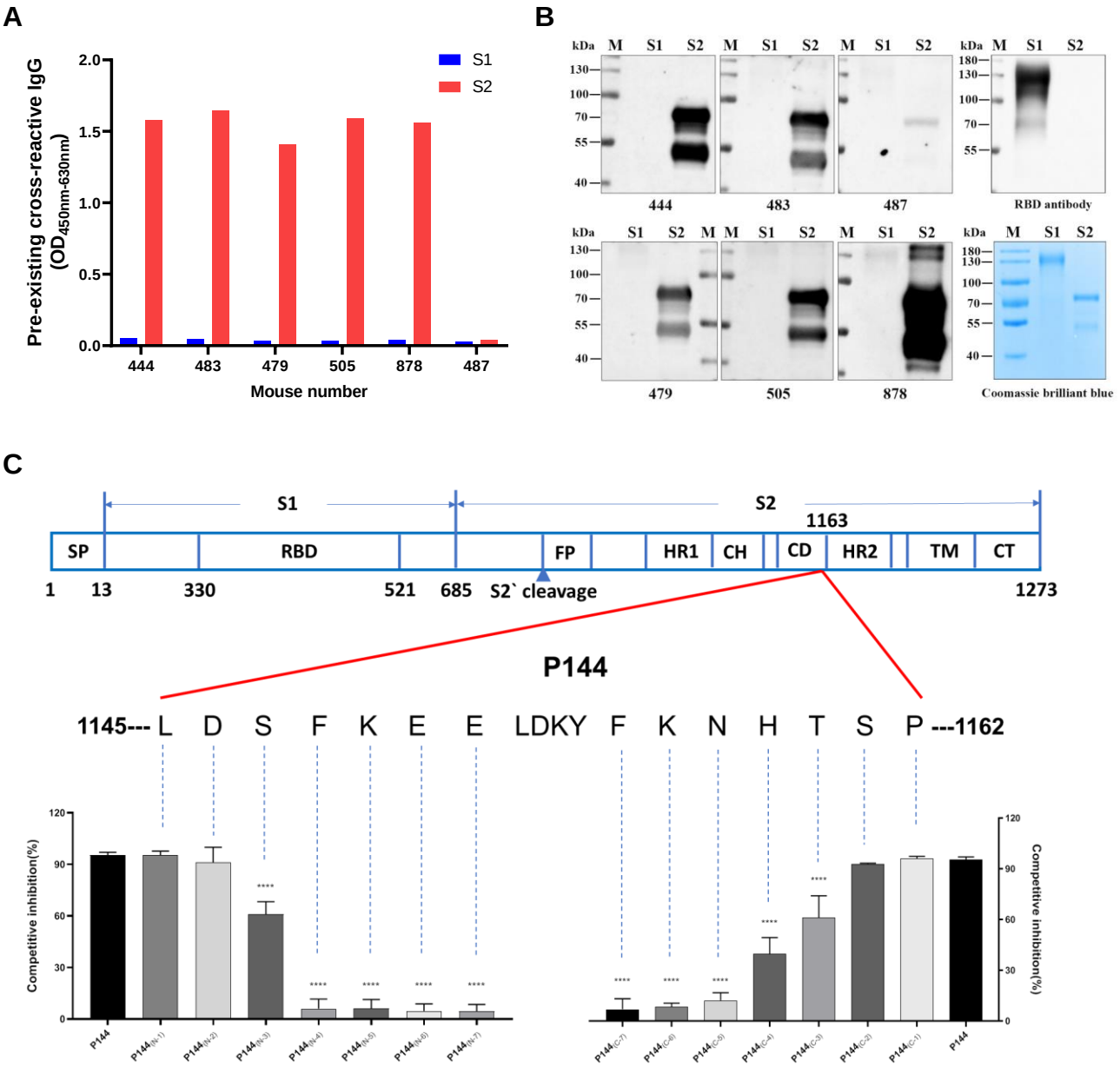

Figure 2 The pre-existing S protein binding antibodies in naïve SPF mice recognized S2 exclusively and a dominant linear antibody epitope was identified on the connector domain. (**A**) The pre-existing S1 and S2 reactive antibody levels in the sera of 6 representative mice. (**B**) WB assays of pre-existing cross-reactive antibodies for 6 representative mouse serum samples. The purities of S1 and S2 proteins were shown by coomassie blue staining. (**C**) The minimal epitope of P144 was defined using a method of competitive ELISA (Data shown as mean±SD, n=5). Purified S2 protein was used as the coating antigen and truncated peptides derived from P144 were used as competitors. The decreases of competitive inhibition reflected the necessity of each amino acid for the epitope recognition. Statistical differences among groups was analyzed using One-way ANOVA. ****, P<0.0001. M: molecular weight marker; SP, signal peptide; RBD, receptor-binding domain; FP, fusion peptide; HR, heptad repeat; CH, central helix; CD, connector domain; TM, transmembrane domain; CT, cytoplasmic tail.

(which was not certified by peer review) is the author/funder, who has granted medRxiv a license to display the preprint in perpetuity.
All rights reserved. No reuse allowed without permission.

Figure 3

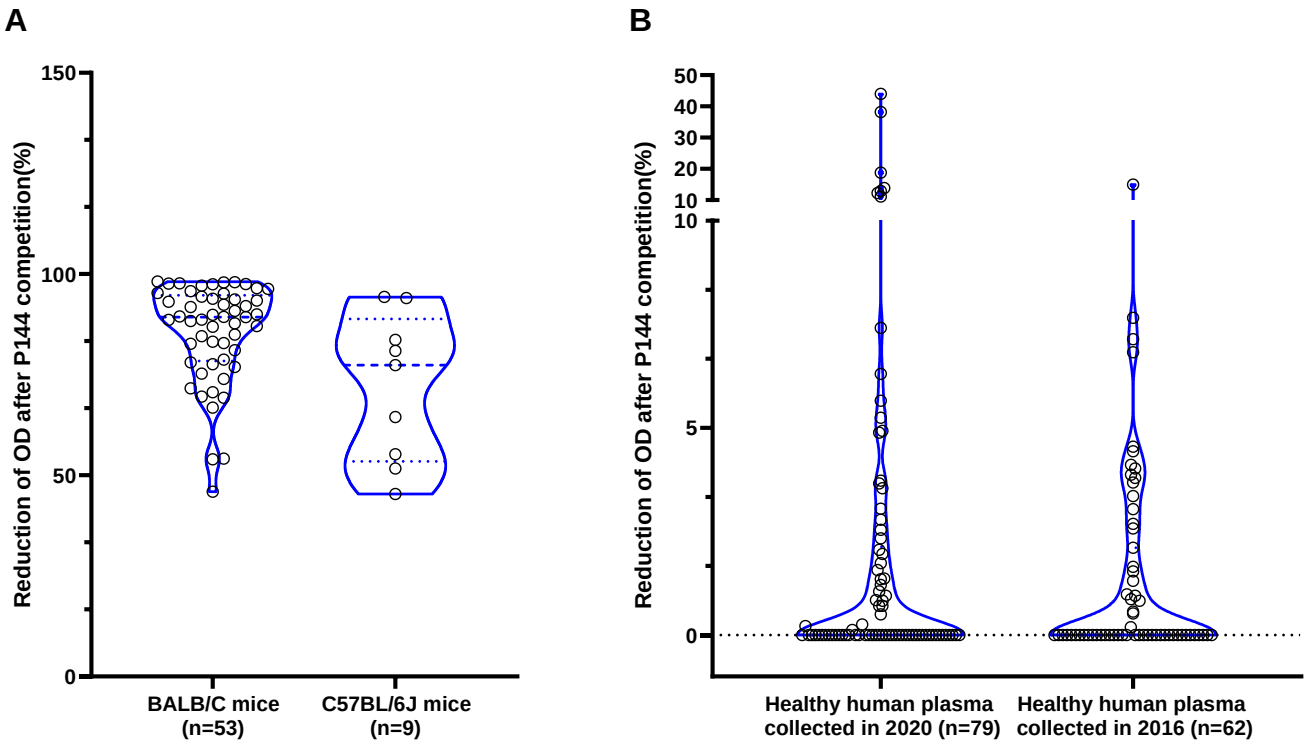

Figure 3 P144 reactive antibodies widely existed in both healthy human and naïve SPF mice. P144 specific binding antibodies were detected using a method of competitive ELISA. (**A**) For the detections of P144 specific binding antibodies in naïve SPF mice, purified S2 protein was used as the coating antigen and P144 peptide was used as the competitor. (**B**) For the detections of P144 specific binding antibodies in healthy individuals, purified BSA-P144 conjugate was used as the coating antigen and P144 peptide was used as the competitor. In both experiments, the reduction of OD value reflected the presence of P144 binding antibodies.

(which was not certified by peer review) is the author/funder, who has granted medRxiv a license to display the preprint in perpetuity.
All rights reserved. No reuse allowed without permission.

Figure 4

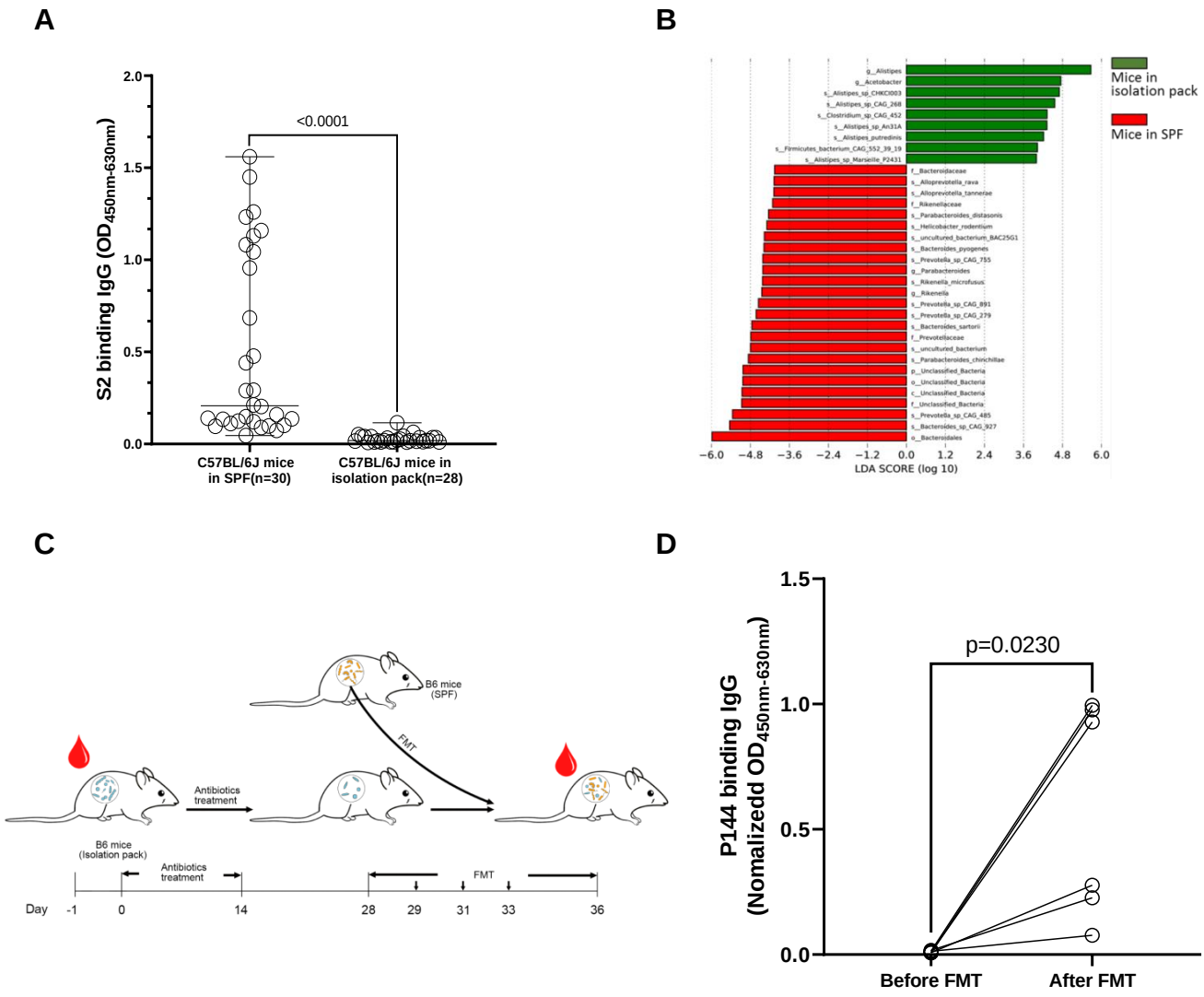

Figure 4 The presence of the pre-existing S2 reactive antibodies was associated with commensal gut bacteria. (A) Comparison of the levels of S2 reactive antibodies between naïve mice maintained under SPF condition and mice housed in a sterile isolation pack. **(B)** Metagenomic analyses of gut microbiota compositions between mice from different housing environments. Differences of bacterial abundance were manifested by linear discriminant analysis (LDA) . **(C)** Schematic overview of the fecal bacteria transplantation (n=6). The mice bred in a sterile isolation pack were treated with a mixture of ampicillin (1g/L), metronidazole (0.5g/L), vancomycin (0.5g/L) and gentamycin (0.5g/L) dissolved in drinking water supplemented with D-glucose (36.8g/L) for 14 days. Two weeks later, fecal bacteria were freshly prepared from SPF mice and delivered to antibiotic treated mice via oral gavage. **(D)** Comparison of P144 reactive antibodies in mouse sera collected before and after FMT. The OD value of P144 binding antibody was normalized to the concentration of total IgG for each mouse. Data are shown as mean±SD (n=6). Statistical analyses were performed by the method of paired t-test. (p), Phylum. (c), Class. (o), Order. (f), Family. (g), Genus. (s), Species.

(which was not certified by peer review) is the author/funder, who has granted medRxiv a license to display the preprint in perpetuity.
All rights reserved. No reuse allowed without permission.

Figure 5

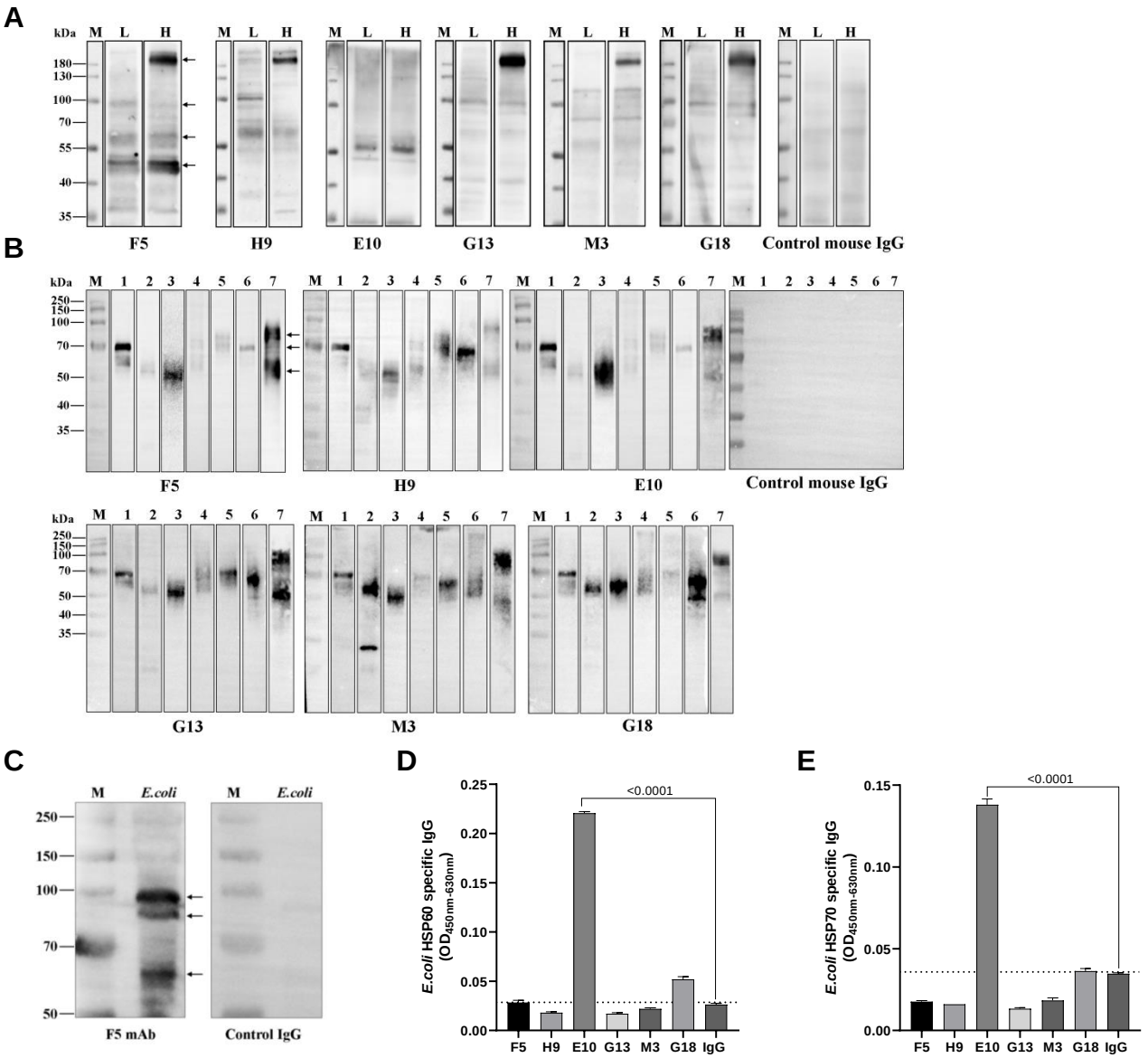

Figure 5 P144 binding mAbs isolated from naïve SPF mice reacted with commensal gut bacteria from both human and mouse. Reactivities between P144 binding mAbs and gut microbial antigens were detected using WB assays. A purified mouse IgG was used as the control. (**A**) WB assays of mouse fecal bacteria samples. L: mixed fecal bacteria samples collected from 3 mice with low levels of pre-existing S2 binding antibodies ($OD_{450nm-630nm}$≤0.140, 1:100 diluted); H: mixed fecal bacteria samples collected from 3 mice with high levels of pre-existing S2 binding antibodies ($OD_{450nm-630nm}$≥0.615, 1:100 diluted). (**B**) WB assays of fecal bacteria samples collected from 7 healthy individuals (Lanes 1-7). All the mAbs and the control mouse IgG were tested at the final concentration of 1μg/ml. Black arrows indicate the locations of protein bands selected for the mass spectrometry analysis. (**C**) Reactivity between a P144 specific mAb (clone F5) and *E. coli* was validated by WB. F5 or a purified mouse IgG was used as the first antibody at the concentration of 1 μg/ml. Black arrows point out the bands with MWs equal to *E. coli* proteins identified by LC-MS analysis. (**D**) Recognition of purified *E.coli* HSP60 protein by P144 reactive antibodies. (**E**) Recognition of purified *E.coli* recombinant HSP70 protein by P144 reactive antibodies. All the mAbs and control IgG were measured at a final concentration of 10 μg/ml. Dotted line represents the mean OD value of control IgG plus 2-fold SD (mean+2SD).

(which was not certified by peer review) is the author/funder, who has granted medRxiv a license to display the preprint in perpetuity.
All rights reserved. No reuse allowed without permission.

Figure 6

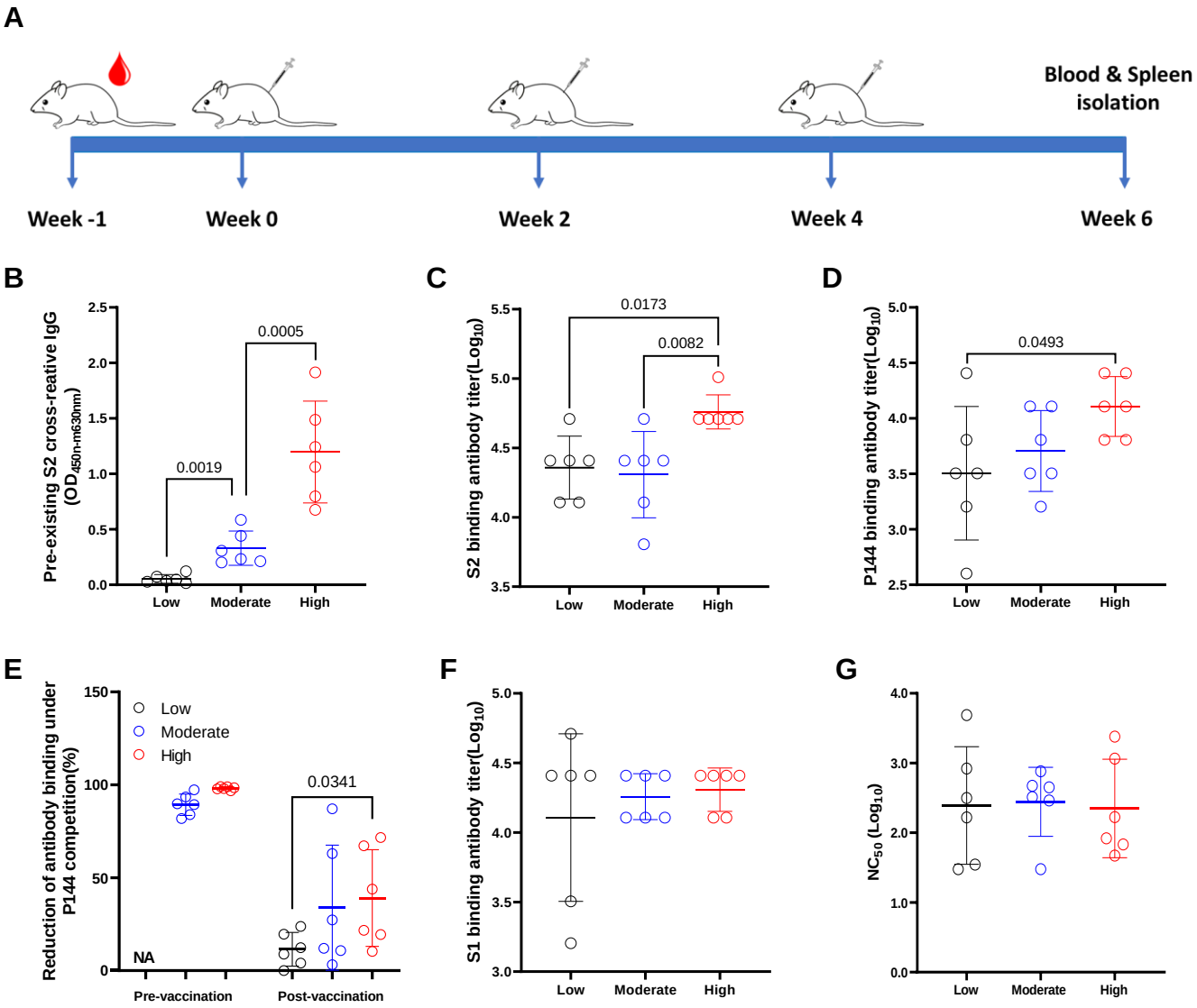

Figure 6 Impacts of pre-existing antibodies on the humoral immune responses elicited by a DNA vaccine encoding SARS-CoV-2 S protein. (**A**) Schematic illustration of the experiment schedule. 50μg of the DNA vaccine was injected intra muscularly into each mice at week 0, week 2 and week 4, respectively. Two weeks after the final vaccination, the mice was euthanized for the measurements of specific immune responses. (**B**) Peripheral blood was collected before immunization and levels of pre-existing S2 specific antibodies were compared among groups. (**C**) Endpoint IgG titers against S2 were compared at 2 weeks post the last immunization. (**D**) Comparisons of P144 specific IgG titers as measured using BSA-P144 conjugate as the coating antigen. (**E**) Comparisons of P144 specific binding antibody levels as determined using a method of competitive ELISA. (**F**) Endpoint IgG titers against S1 measured at 2 weeks post the final vaccination. (**G**) Neutralizing antibody titers against SARS-CoV-2 D614G pseudo-virus in serum of mice at 2 weeks post the final immunization. Data were shown as mean±SD, n=6. Statistical analyses were performed by the method of one-way ANOVA.

(which was not certified by peer review) is the author/funder, who has granted medRxiv a license to display the preprint in perpetuity.
All rights reserved. No reuse allowed without permission.

Figure 7

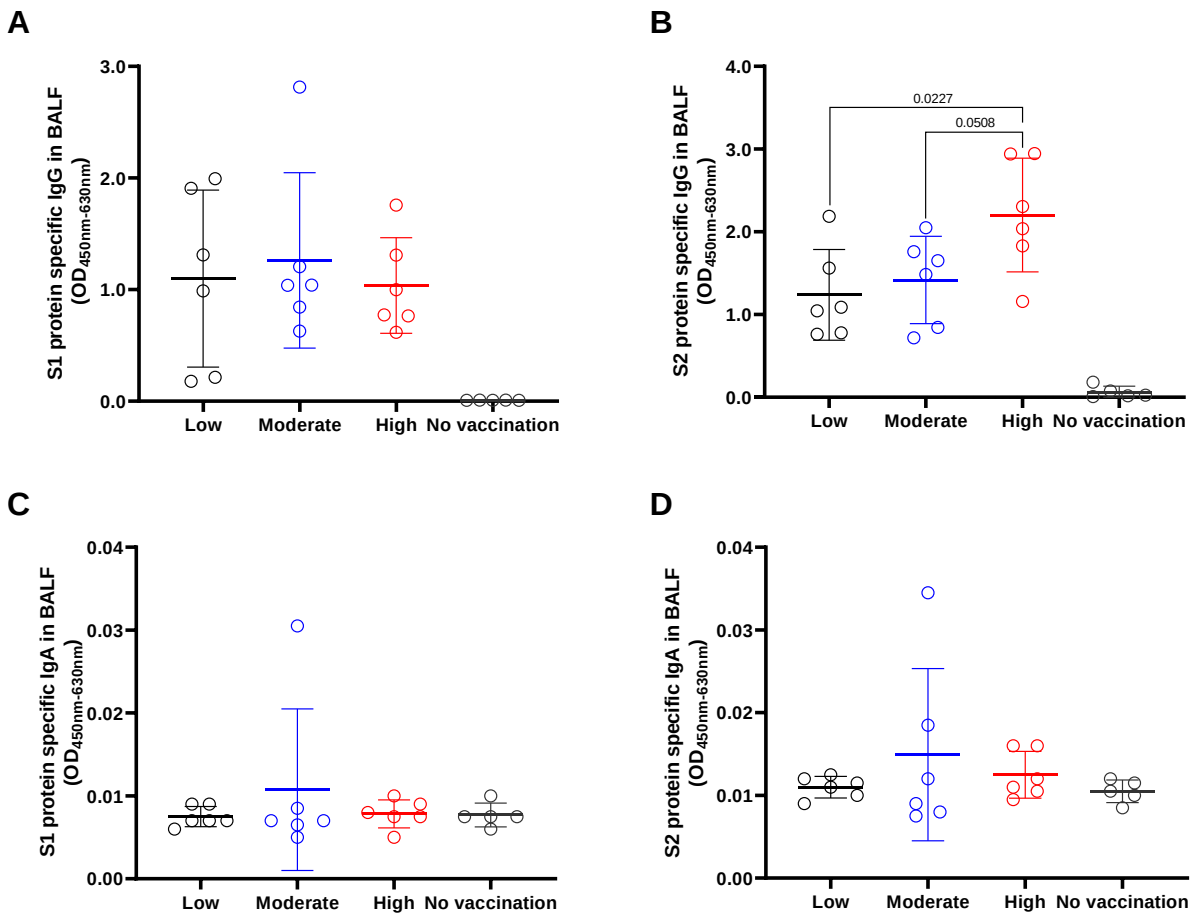

Figure 7 The impacts of pre-existing antibody on the levels of specific IgG and IgA in BALF after vaccination. BALF was collected from each mouse after euthanasia. Specific IgG (**A** and **B**) and IgA (**C** and **D**) against S1 or S2 were detected using in-house ELISA methods. All the BALF samples were adjusted to the initial total protein concentration of 51.9μg/ml. Data are shown as mean±SD, n=6. Statistical analyses were performed by the method of one-way ANOVA.

(which was not certified by peer review) is the author/funder, who has granted medRxiv a license to display the preprint in perpetuity.
All rights reserved. No reuse allowed without permission.

Figure 8

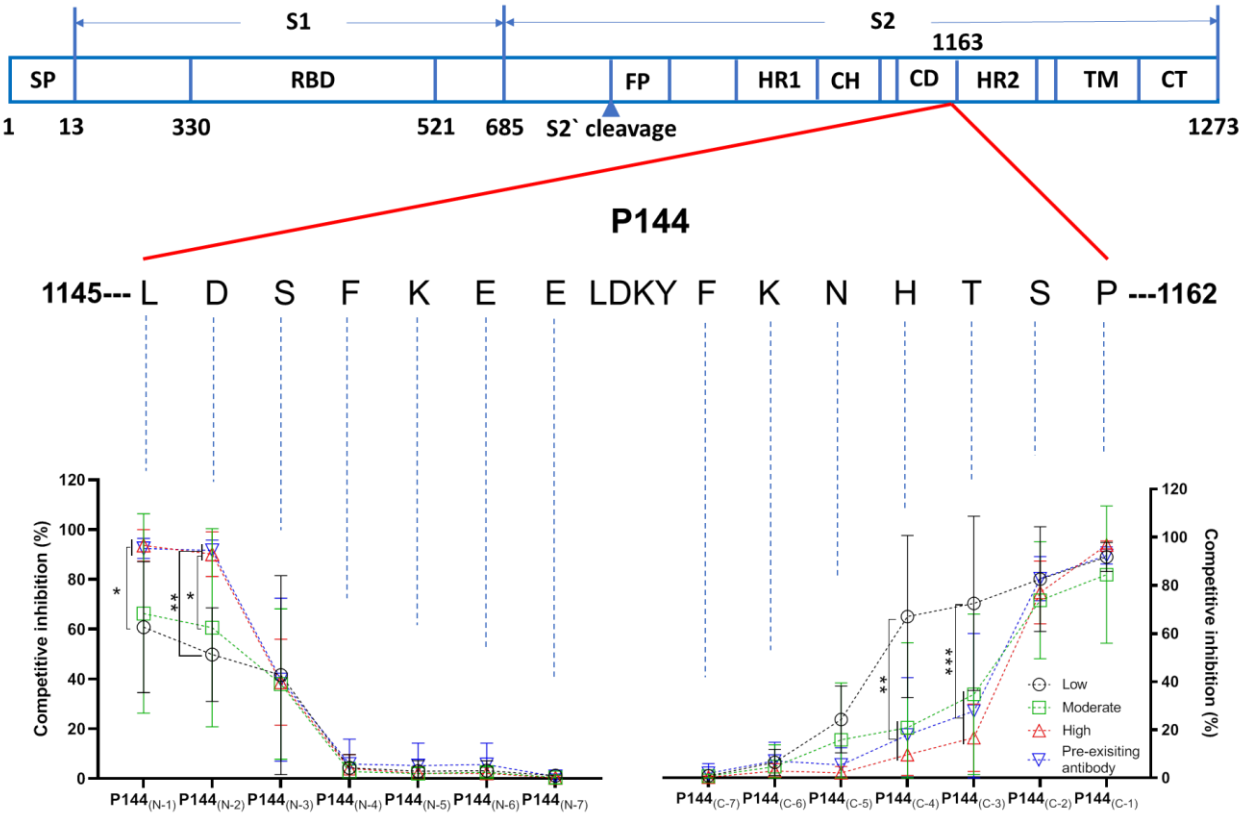

Figure 8 The impact of pre-existing antibody on the recognition of the minimum epitope of P144 after vaccination. The minimal epitope recognized by mouse sera after vaccination was analyzed using a method of competitive ELISA. Purified BSA-P144 conjugate was used as the coating antigen and truncated peptides derived from P144 were used as the competitors. The decreases of competitive inhibition reflected the necessity of each amino acid for the epitope recognition. Statistical analyses were performed by the method of two-tailed t-test (*, $P< 0.05$, **, $P< 0.01$, ***, $P< 0.001$).

(which was not certified by peer review) is the author/funder, who has granted medRxiv a license to display the preprint in perpetuity.
All rights reserved. No reuse allowed without permission.

Figure 9

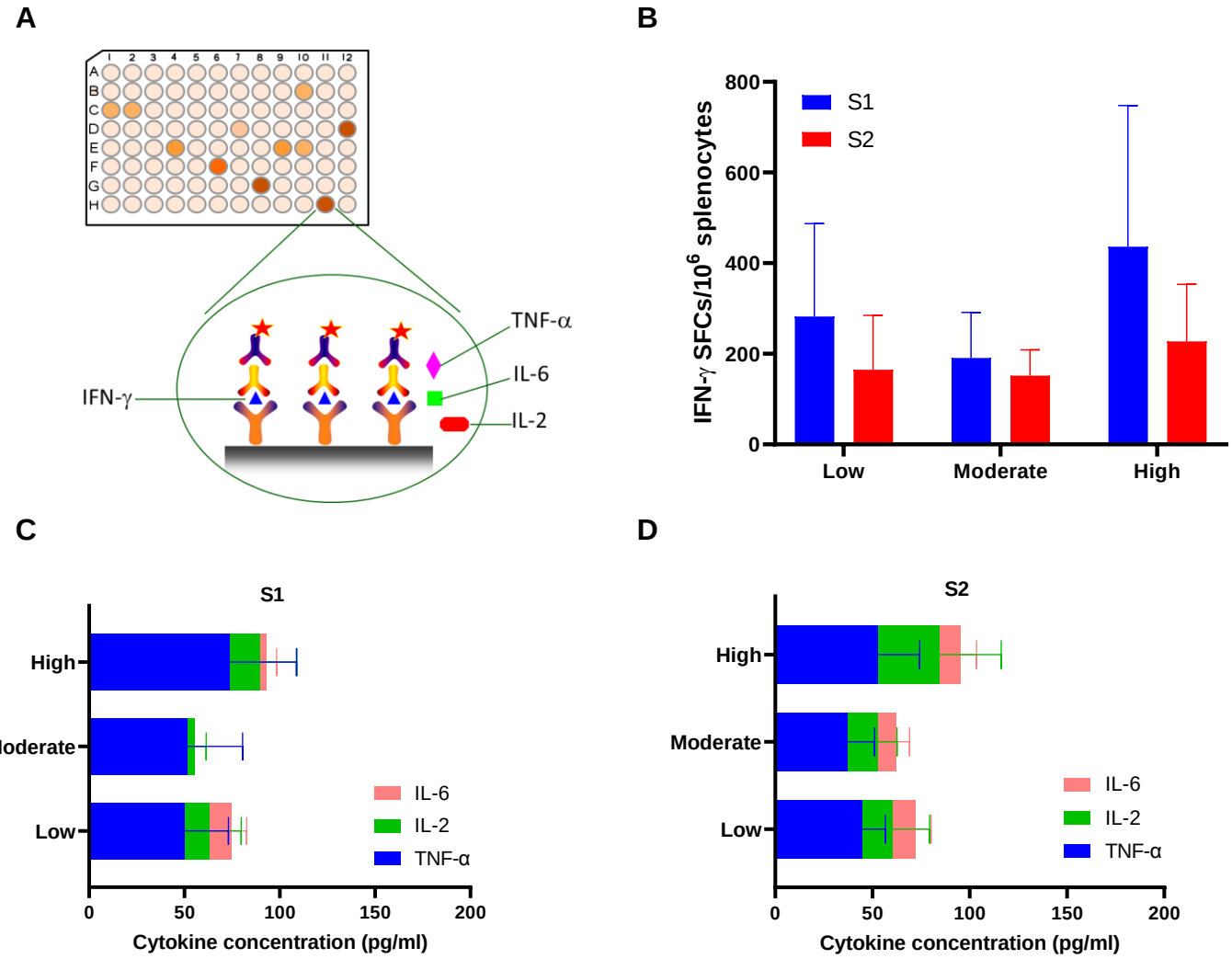

Figure 9 The impacts of pre-existing antibody on the cellular immune responses after vaccination. (**A**) The diagram of the method used for cellular immune responses evaluation. (**B**) S1 and S2 specific IFN-γ responses were compared among groups of mice with different levels of pre-existing S2 reactive antibodies. Additionally, S1 (**C**) and S2 (**D**) specific releases of IL-2, IL-6 and TNF-α as measured using the method of multiplex cytokine bead assay were also compared among different groups. Data were shown as mean± SD, n=6. SFCs, spot forming cells.

(which was not certified by peer review) is the author/funder, who has granted medRxiv a license to display the preprint in perpetuity.
All rights reserved. No reuse allowed without permission.

Figure 10

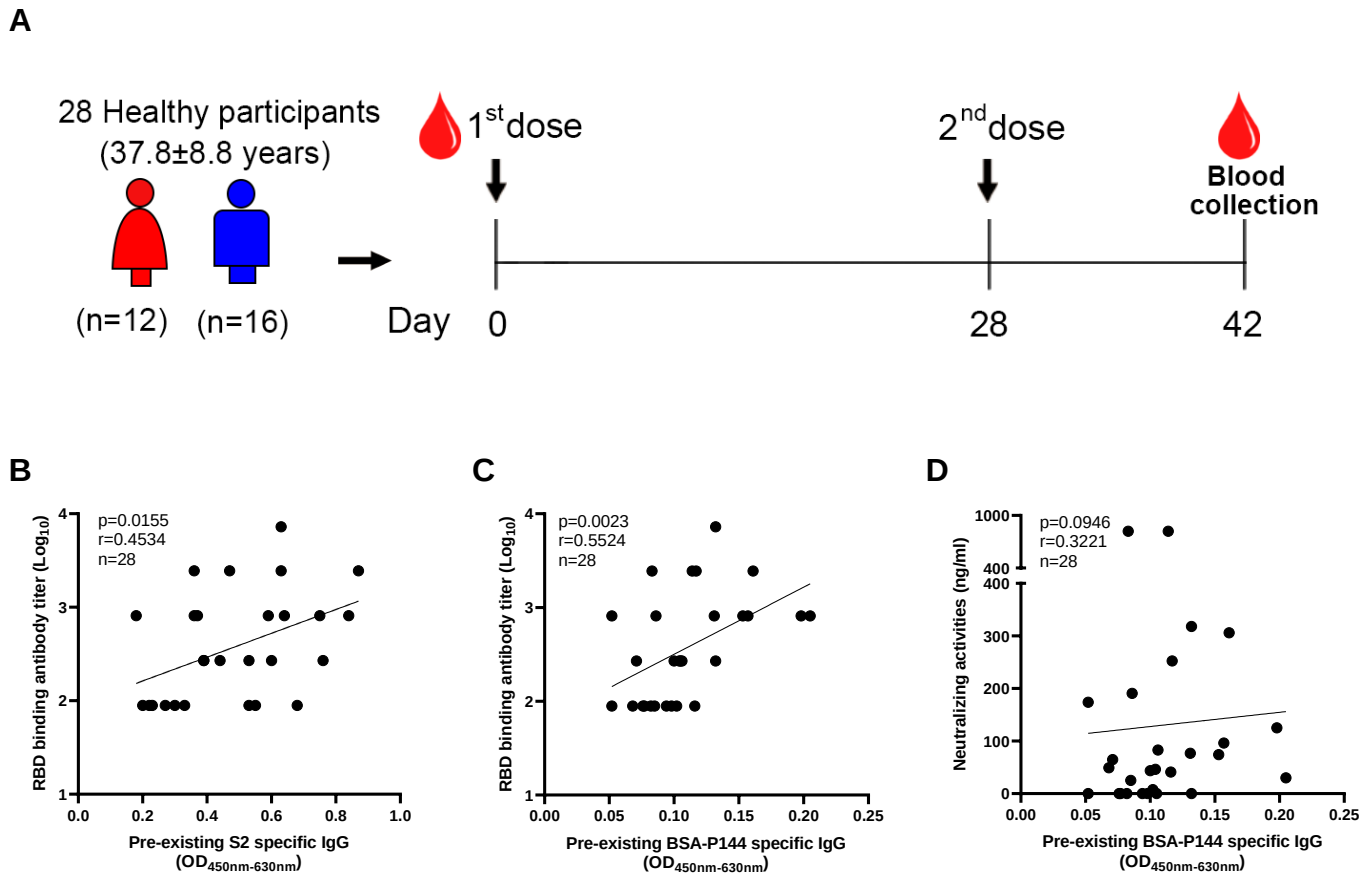

Figure 10 Levels of pre-existing S2 reactive antibodies correlated with RBD binding antibody responses elicited by an inactivated SARS-CoV-2 vaccine in human. (A) Peripheral blood samples were collected from 28 healthy vaccines who received two doses of an inactivated SARS-CoV-2 vaccine at baseline and 14 days post the 2nd dose, respectively. The RBD binding antibody titers were measured by ELISA. The neutralizing antibody responses were quantified by a commercialized surrogate virus neutralization test (sVNT) (Suzhou Sym-Bio Life Science Co., Ltd). **(B and C**) Correlations between RBD binding antibody titers and levels of pre-existing S2 or P144 specific IgG. **(D)** Correlation between neutralizing antibody concentrations and pre-existing P144 binding antibody levels. Statistical analyses were performed using the method of Spearman's correlation**.** The experiment was repeated twice.

medRxiv preprint doi: https://doi.org/10.1101/2021.07.13.21260404; this version posted January 21, 2022. The copyright holder for this preprint (which was not certified by peer review) is the author/funder, who has granted medRxiv a license to display the preprint in perpetuity.
All rights reserved. No reuse allowed without permission.

Table 1 Demographics of SARS-CoV-2 unexposed healthy individuals

Sample Collection Time	**2016**	**2020**
Number of individuals	78	95
Gender (males, females)	17, 61	78, 17
Age, years (mean ± SD)	35.88 ± 8.40	30.40 ± 7.55

Table 2 Potential cross-reactive antigens identified in mouse fecal bacteria

NCBI Accession #	Protein name	Bacterium	Score	Proteins	Unique Peptides	Peptides	PSMs	Area	MW [kDa]
Q8A470	DNA-directed RNA polymerase subunit beta' OS	Bacteroides thetaiotaomicron	168.01	550	2	6	6	3.536E7	158.3
Q5L897	DNA-directed RNA polymerase subunit beta OS	Bacteroides fragilis	92.15	8	2	3	3	8.315E6	142.4
Q8A1G1	TonB-dependent receptor SusC OS	Bacteroides thetaiotaomicron	145.74	1	1	2	3	1.385E8	111.1
Q46509	Aldehyde oxidoreductase OS	Desulfovibrio gigas	75.93	1	1	1	1	8.506E6	97.0
P22983	Pyruvate, phosphate dikinase OS	Clostridium symbiosum	109.83	7	2	2	2	3.721E7	96.6
P0A9Q8	Aldehyde-alcohol dehydrogenase OS	Escherichia coli	34.29	1	1	1	1	1.085E7	96.1
Q826F6	Chaperone protein dnaK2 OS	Streptomyces avermitilis	20.37	1	1	1	1	1.059E7	67.5
Q892R0	Chaperone protein DnaK OS	Clostridium tetani	51.52	5	1	1	1	1.780E7	66.4
B1I9W8	L-fucose isomerase OS	Streptococcus pneumoniae	57.33	12	2	2	2	2.792E7	65.7
P95334	Chaperone protein DnaK OS	Myxococcus xanthus	39.23	4	1	1	1	1.792E7	65.3
Q1MPZ9	Formate--tetrahydrofolate ligase OS	Lawsonia intracellularis	62.49	1	2	2	2	2.068E7	64.2
P26929	Urease subunit alpha OS	Lactobacillus fermentum	134.06	4	4	4	5	1.526E7	61.8
Q9I165	Periplasmic trehalase OS	Pseudomonas aeruginosa	77.05	1	1	1	1	4.240E8	61.1
Q9EZ02	Pyrophosphate--fructose 6-phosphate 1-phosphotransferase OS	Spirochaeta thermophila	68.21	2	1	1	1	1.192E7	61.0
P14407	Fumarate hydratase class I, anaerobic OS	Escherichia coli	30.79	1	1	1	1	6.580E6	60.1
Q189R2	Formate--tetrahydrofolate ligase OS	Clostridioides difficile	123.52	22	3	4	4	2.621E7	59.9
P22252	Flagellin B OS	Campylobacter jejuni subsp. jejuni serotype O:6	75.42	1	1	1	1	1.478E7	59.7
Q1WTW0	Formate--tetrahydrofolate ligase OS	Lactobacillus salivarius	83.43	23	1	1	1	5.229E7	59.4
A7HLZ4	Formate--tetrahydrofolate ligase OS	Fervidobacterium nodosum	93.49	29	1	2	2	8.036E6	59.2
C4ZBL1	Phosphoenolpyruvate carboxykinase (ATP) OS	Agathobacter rectalis	211.34	4	1	4	5	3.965E7	59.0
A6LFQ4	Phosphoenolpyruvate carboxykinase (ATP) OS	Parabacteroides distasonis	32.29	1	1	1	1	8.523E6	58.9
A3MZI4	Formate--tetrahydrofolate ligase OS	Actinobacillus pleuropneumoniae serotype 5b	78.45	78	1	2	2	1.320E8	58.9
Q2LPJ8	60 kDa chaperonin 1 OS	Syntrophus aciditrophicus	101.22	15	1	2	3	2.217E7	58.6
Q3ALZ3	60 kDa chaperonin 1 OS	Synechococcus sp.	113.34	23	1	2	3	9.973E7	58.5
B8J123	60 kDa chaperonin OS	Desulfovibrio desulfuricans	232.59	27	2	5	6	9.659E7	58.4
Q72AL6	60 kDa chaperonin OS	Desulfovibrio vulgaris	126.02	9	1	3	3	2.402E7	58.4

medRxiv preprint doi: https://doi.org/10.1101/2021.07.13.21260404; this version posted January 21, 2022. The copyright holder for this preprint (which was not certified by peer review) is the author/funder, who has granted medRxiv a license to display the preprint in perpetuity.
All rights reserved. No reuse allowed without permission.

A0Q2T1	60 kDa chaperonin OS	Clostridium novyi	78.78	16	1	2	2	2.292E7	58.1
B0SCC0	60 kDa chaperonin OS	Leptospira biflexa serovar Patoc	49.58	1	1	1	1	1.882E8	58.1
B2TIX0	60 kDa chaperonin OS	Clostridium botulinum	126.34	35	1	3	3	4.903E7	57.9
A7GZ43	60 kDa chaperonin OS	Campylobacter curvus	105.05	41	2	3	3	5.327E7	57.9
Q67KB8	60 kDa chaperonin OS	Symbiobacterium thermophilum	107.47	126	1	3	3	9.411E7	57.9
B5YDR9	60 kDa chaperonin OS	Dictyoglomus thermophilum	59.61	2	1	1	1	3.345E7	57.9
Q3ADX3	60 kDa chaperonin OS	Carboxydothermus hydrogenoformans	104.07	25	1	2	3	7.715E7	57.6
O50305	60 kDa chaperonin OS	Bacillus halodurans	250.57	55	3	4	6	3.021E8	57.4
P26821	60 kDa chaperonin OS	Clostridium perfringens	131.27	36	1	3	3	4.609E7	57.3
P37282	60 kDa chaperonin OS	Lactococcus lactis subsp. lactis	102.15	18	1	2	2	4.298E7	57.2
C4ZD46	60 kDa chaperonin OS	Agathobacter rectalis	372.10	52	3	5	8	3.352E8	57.1
A6L8C4	Glucose-6-phosphate isomerase OS	Parabacteroides distasonis	88.85	55	1	2	3	5.392E8	48.7
P43793	NADP-specific glutamate dehydrogenase OS	Haemophilus influenzae	96.32	2	1	2	2	7.357E7	48.6
P00370	NADP-specific glutamate dehydrogenase OS	Escherichia coli	161.88	1	1	3	4	3.280E8	48.6
P15111	NADP-specific glutamate dehydrogenase OS	Salmonella typhimurium	185.28	4	1	4	5	1.755E8	48.5
P94316	NAD-specific glutamate dehydrogenase OS	Bacteroides fragilis	192.93	3	3	5	6	1.730E8	48.4
Q1WSY0	Enolase OS	Lactobacillus salivarius	79.89	8	3	3	3	1.340E7	48.0
B7MD95	Trigger factor OS	Escherichia coli O45:K1	78.80	10	2	2	2	4.344E7	47.8
B2GAM0	Enolase OS	Lactobacillus fermentum	79.94	8	2	2	2	1.858E7	47.8
Q6MEY2	Enolase OS	Protochlamydia amoebophila	112.67	1	1	1	1	7.493E7	47.5
Q0SNH5	Enolase OS	Borrelia afzelii	71.86	2	1	1	1	4.654E7	47.4
G3KIM4	Lactoyl-CoA dehydratase subunit alpha (Fragment) OS	Anaerotignum propionicum	63.03	1	1	1	1	1.136E7	47.4
Q9I3S1	Biofilm dispersion protein BdlA OS	Pseudomonas aeruginosa	59.07	22	1	1	1	3.282E7	46.9
B8J4A8	Sulfate adenylyltransferase OS	Desulfovibrio desulfuricans	210.65	1	5	5	5	2.656E7	46.9
A6L3M9	Enolase OS	Bacteroides vulgatus	48.62	2	1	2	2	3.004E7	46.7
Q043Z5	Enolase 1 OS	Lactobacillus gasseri	289.72	4	5	5	5	4.189E7	46.6
Q1ISS7	Enolase OS	Koribacter versatilis	71.57	4	1	1	1	7.884E6	46.5
B8DTI9	Enolase OS	Bifidobacterium animalis subsp. lactis	115.71	4	2	2	2	1.684E7	46.4
A7GUR7	Enolase OS	Bacillus cytotoxicus	122.68	17	2	2	3	2.771E7	46.4
Q2LR33	Enolase OS	Syntrophus aciditrophicus	31.73	1	1	1	1	4.823E7	46.2
Q89Z05	Enolase OS	Bacteroides thetaiotaomicron	140.16	2	2	4	5	3.005E7	46.1

medRxiv preprint doi: https://doi.org/10.1101/2021.07.13.21260404; this version posted January 21, 2022. The copyright holder for this preprint (which was not certified by peer review) is the author/funder, who has granted medRxiv a license to display the preprint in perpetuity.
All rights reserved. No reuse allowed without permission.

B2RLL7	Enolase OS	Porphyromonas gingivalis	123.91	2	2	3	3	2.636E7	45.8
Q6MPQ2	Enolase OS	Bdellovibrio bacteriovorus	66.50	1	1	1	1	8.918E6	45.7
B0K742	Serine hydroxymethyltransferase OS	Thermoanaerobacter pseudethanolicus	85.67	92	2	2	2	2.140E7	45.6
Q5LFT7	Peptidase T OS	Bacteroides fragilis	89.56	5	1	1	1	7.323E7	45.5
A9NEA9	Serine hydroxymethyltransferase OS	Acholeplasma laidlawii	44.82	3	1	1	1	5.875E6	45.3
Q7MU77	Phosphoglycerate kinase OS	Porphyromonas gingivalis	54.70	1	1	1	1	2.106E7	45.0
Q8A753	Phosphoglycerate kinase OS	Bacteroides thetaiotaomicron	25.30	1	1	1	1	1.320E7	45.0
A5VHR0	Phosphopentomutase OS	Lactobacillus reuteri	159.08	1	4	4	4	4.364E7	44.0
A8EWM4	Phosphoglycerate kinase OS	Arcobacter butzleri	45.52	1	1	1	1	2.577E7	43.8
Q042T5	Elongation factor Tu OS	Lactobacillus gasseri	400.92	36	3	10	13	1.184E8	43.7
Q74JU6	Elongation factor Tu OS	Lactobacillus johnsonii	348.06	36	2	9	12	1.184E8	43.6
Q5L890	Elongation factor Tu OS	Bacteroides fragilis	185.88	297	3	5	7	1.454E8	43.6
Q8R603	Elongation factor Tu OS	Fusobacterium nucleatum subsp. nucleatum	150.02	302	1	3	3	6.170E7	43.4
B8J1A0	Elongation factor Tu OS	Desulfovibrio desulfuricans	139.50	64	2	3	3	4.287E7	43.4
A5VJ92	Elongation factor Tu OS	Lactobacillus reuteri	413.79	60	8	11	13	3.595E8	43.4

Note: *Score:* The Mascot score. Proteins: The total number of proteins contained in the protein group. *Unique Peptides:* The total number of peptides unique to the protein group. *Peptides:* The total number of peptides identified from all included searches for the master protein of the protein group. *PSMs:* The total number of peptide-spectrum matches identified from all included searches for the master protein of the protein group. *Area:* The chromatographic peak area was used to characterize the quantitative abundance of protein.*MW(kDa):* The theoretical molecular weight of the protein.

medRxiv preprint doi: https://doi.org/10.1101/2021.07.13.21260404; this version posted January 21, 2022. The copyright holder for this preprint (which was not certified by peer review) is the author/funder, who has granted medRxiv a license to display the preprint in perpetuity. All rights reserved. No reuse allowed without permission.

Table 3 Potential cross-reactive antigens identified in human fecal bacteria

NCBI Accession #	Protein Name	Bacterium	Score	Proteins	Unique Peptides	Peptides	PSMs	Area	MW [kDa]
A6LFK9	Polyribonucleotide nucleotidyltransferase OS	Parabacteroides distasonis	62.68	3	1	2	2	2.332E7	82.0
P75764	Uncharacterized protein YbhJ OS	Escherichia coli	27.35	1	1	1	1	3.198E7	81.5
Q8A4N6	Polyribonucleotide nucleotidyltransferase OS	Bacteroides thetaiotaomicron	226.97	23	6	7	7	6.947E7	78.3
B3DT30	Elongation factor G OS	Bifidobacterium longum	236.98	64	8	10	11	4.407E7	78.1
E1WNR6	Chaperone protein htpG OS	Bacteroides fragilis	131.15	4	1	2	2	4.992E7	77.9
O31673	ATP-dependent Clp protease ATP-binding subunit ClpE OS	Bacillus subtilis	120.19	73	1	3	4	8.448E7	77.9
A7ZSL5	Elongation factor G OS	Escherichia coli O139:H28	133.81	92	2	3	4	2.888E7	77.5
Q5L8A7	Elongation factor G OS	Bacteroides fragilis	431.35	187	3	10	14	1.391E8	77.5
A6KYJ7	Elongation factor G OS	Bacteroides vulgatus	361.61	186	2	9	12	1.342E8	77.4
A6LFP0	Methionine--tRNA ligase OS	Parabacteroides distasonis	65.86	8	1	1	1	4.772E7	77.4
P39396	Pyruvate/proton symporter BtsT OS	Escherichia coli	92.20	1	2	2	2	1.446E7	77.3
A9KNK6	Polyribonucleotide nucleotidyltransferase OS	Lachnoclostridium phytofermentans	68.87	1	1	1	1	1.075E8	76.9
Q5L6S5	Elongation factor G OS	Chlamydia abortus	76.05	58	1	2	3	1.622E7	76.8
Q67JU0	Elongation factor G OS	Symbiobacterium thermophilum	147.39	86	1	4	5	2.631E8	76.8
Q5U8S9	Elongation factor G OS	Staphylococcus intermedius	98.88	65	1	3	4	5.177E7	76.7
Q8A294	Putative K(+)-stimulated pyrophosphate-energized sodium pump OS	Bacteroides thetaiotaomicron	150.65	20	1	3	3	1.276E8	76.5
B9DYA6	Elongation factor G OS	Clostridium kluyveri	136.00	67	1	3	4	8.826E7	76.4
Q5WLR5	Elongation factor G OS	Bacillus clausii	134.85	81	1	4	5	1.119E8	76.4
Q97I51	Translation initiation factor IF-2 OS	Clostridium acetobutylicum	70.53	4	1	1	1	2.330E8	76.3
A0PXU3	Elongation factor G OS	Clostridium novyi	114.21	67	1	3	4	8.905E7	76.1
Q18CF4	Elongation factor G OS	Clostridioides difficile	174.49	59	1	4	5	1.288E8	75.8
Q8AB53	Putative glucosamine-6-phosphate deaminase-like protein BT_0258 OS	Bacteroides thetaiotaomicron	54.10	1	1	1	1	4.629E6	75.2
Q8XJ01	Penicillin-binding protein 1A OS	Clostridium perfringens	39.66	3	1	1	1	1.599E7	75.1
A6L7J7	Threonine--tRNA ligase OS	Bacteroides vulgatus	91.33	9	2	2	2	2.440E7	74.2
P30539	1,4-alpha-glucan branching enzyme GlgB OS	Butyrivibrio fibrisolvens	30.12	1	1	1	1	2.287E7	73.8
B2TIT5	Threonine--tRNA ligase OS	Clostridium botulinum	53.61	2	1	1	1	1.877E7	73.8

medRxiv preprint doi: https://doi.org/10.1101/2021.07.13.21260404; this version posted January 21, 2022. The copyright holder for this preprint (which was not certified by peer review) is the author/funder, who has granted medRxiv a license to display the preprint in perpetuity. All rights reserved. No reuse allowed without permission.

P56116	Chaperone protein HtpG OS	Helicobacter pylori	38.02	12	1	1	1	1.269E7	71.2
P0A9P7	ATP-dependent RNA helicase DeaD OS	Escherichia coli O6:H1	85.88	5	3	3	4	1.336E8	70.5
P19410	3-oxocholoyl-CoA 4-desaturase OS	Clostridium scindens	63.87	1	1	1	1	5.844E7	70.2
Q8RHJ2	Putative K(+)-stimulated pyrophosphate-energized sodium pump OS	Fusobacterium nucleatum subsp. nucleatum	140.41	23	1	3	3	1.320E8	68.9
A5CX56	Chaperone protein DnaK OS	Vesicomyosocius okutanii subsp. Calyptogena okutanii	15.38	1	1	1	1	2.961E7	68.7
Q5LG30	Chaperone protein DnaK OS	Bacteroides fragilis	418.39	33	1	9	11	6.399E7	68.6
Q89YW6	Chaperone protein DnaK OS	Bacteroides thetaiotaomicron	372.24	35	1	7	9	6.399E7	68.3
A6L2X7	Chaperone protein DnaK OS	Bacteroides vulgatus	371.71	33	1	8	10	6.399E7	68.3
Q93GF1	Chaperone protein DnaK OS	Prevotella loescheii	185.46	1	4	4	4	3.512E7	68.0
A6LGR5	4-hydroxy-3-methylbut-2-en-1-yl diphosphate synthase (flavodoxin) OS	Parabacteroides distasonis	38.34	5	1	1	1	2.396E7	67.9
B8H444	ATP-dependent zinc metalloprotease FtsH OS	Caulobacter vibrioides	26.45	6	1	1	1	1.241E7	67.7
A9KIA6	Aspartate--tRNA(Asp/Asn) ligase OS	Lachnoclostridium phytofermentans	31.12	1	1	1	1	8.400E6	67.5
P0AG91	Protein translocase subunit SecD OS	Escherichia coli O157:H7	233.70	2	6	6	6	2.164E7	66.6
Q49Y22	Chaperone protein DnaK OS	Staphylococcus saprophyticus subsp. saprophyticus	56.64	206	1	2	2	1.171E7	66.5
A6LBU6	Aspartate--tRNA ligase OS	Parabacteroides distasonis	88.06	49	1	2	2	7.901E6	66.4
P21332	Oligo-1,6-glucosidase OS	Bacillus cereus	53.99	2	1	1	1	1.391E7	66.0
Q8A5W4	Lysine--tRNA ligase OS	Bacteroides thetaiotaomicron	154.84	2	2	2	2	1.304E7	65.9
Q8GBW6	Methylmalonyl-CoA carboxyltransferase 12S subunit OS	Propionibacterium freudenreichii subsp. shermanii	98.01	1	1	1	2	1.386E8	65.9
Q67S54	Chaperone protein DnaK OS	Symbiobacterium thermophilum	96.29	225	1	3	3	4.528E7	65.7
Q9RQ13	L-fucose isomerase OS	Bacteroides thetaiotaomicron	181.20	7	1	5	7	1.038E8	65.7
A6L048	L-fucose isomerase OS	Bacteroides vulgatus	162.35	5	2	6	7	3.672E7	65.6
Q56403	V-type ATP synthase alpha chain OS	Thermus thermophilus	132.50	30	1	1	2	1.117E7	63.6
Q8G7I6	Glucose-6-phosphate isomerase OS	Bifidobacterium longum	531.07	4	14	14	15	3.155E8	63.0
Q4JX51	Glucose-6-phosphate isomerase OS	Corynebacterium jeikeium	30.85	1	1	1	1	3.306E7	62.1
Q8FZC4	2-isopropylmalate synthase OS	Brucella suis biovar 1	51.65	8	1	1	1	1.014E7	61.6
A6TGT4	Glucose-6-phosphate isomerase OS	Klebsiella pneumoniae subsp. pneumoniae	53.60	21	1	1	1	3.337E7	61.3

medRxiv preprint doi: https://doi.org/10.1101/2021.07.13.21260404; this version posted January 21, 2022. The copyright holder for this preprint (which was not certified by peer review) is the author/funder, who has granted medRxiv a license to display the preprint in perpetuity. All rights reserved. No reuse allowed without permission.

P0AG69	30S ribosomal protein S1 OS	Escherichia coli O157:H7	88.52	1	2	2	2	8.393E6	61.1
Q9EZ02	Pyrophosphate--fructose 6-phosphate 1-phosphotransferase OS	Spirochaeta thermophila	110.07	2	2	2	2	1.245E8	61.0
O31716	Uncharacterized ABC transporter ATP-binding protein YkpA OS	Bacillus subtilis	48.45	1	1	1	1	2.259E6	61.0
P59173	Probable 2,3-bisphosphoglycerate-independent phosphoglycerate mutase OS	Leptospira interrogans serogroup Icterohaemorrhagiae serovar Lai	61.50	2	1	1	2	6.104E6	61.0
P23843	Periplasmic oligopeptide-binding protein OS	Escherichia coli	368.94	2	11	11	12	1.586E8	60.9
Q0SQ82	Formate--tetrahydrofolate ligase OS	Clostridium perfringens	167.47	26	1	3	4	6.063E7	60.4
P14407	Fumarate hydratase class I, anaerobic OS	Escherichia coli	66.46	4	2	2	2	4.922E7	60.1
Q3A9K2	Formate--tetrahydrofolate ligase OS	Carboxydothermus hydrogenoformans	110.68	55	1	3	3	3.356E8	60.1
Q251P8	Formate--tetrahydrofolate ligase 1 OS	Desulfitobacterium hafniense	72.85	55	1	2	2	5.742E8	60.0
C0QX38	Formate--tetrahydrofolate ligase OS	Brachyspira hyodysenteriae	145.04	9	1	2	3	2.562E7	60.0
Q189R2	Formate--tetrahydrofolate ligase OS	Clostridioides difficile	157.46	1	3	3	3	1.347E9	59.9
C4ZBG8	Formate--tetrahydrofolate ligase OS	Agathobacter rectalis	235.86	56	4	6	6	3.610E8	59.7
A8AQV7	Phosphoenolpyruvate carboxykinase (ATP) OS	Citrobacter koseri	104.30	44	4	5	5	1.300E8	59.6
Q24ZZ8	Formate--tetrahydrofolate ligase 2 OS	Desulfitobacterium hafniense	79.67	55	1	2	2	5.193E8	59.4
B2RHV8	Phosphoenolpyruvate carboxykinase (ATP) OS	Porphyromonas gingivalis	188.39	21	2	5	5	2.446E8	59.4
Q47VD0	Phosphoenolpyruvate carboxykinase (ATP) OS	Colwellia psychrerythraea	111.53	16	1	2	2	1.952E8	59.3
A1R7X2	Arginine--tRNA ligase OS	Paenarthrobacter aurescens	43.93	15	1	1	1	2.994E7	59.2
Q8A414	Phosphoenolpyruvate carboxykinase (ATP) OS	Bacteroides thetaiotaomicron	293.03	21	3	8	8	3.939E8	59.1
C4ZBL1	Phosphoenolpyruvate carboxykinase (ATP) OS	Agathobacter rectalis	501.52	17	5	12	15	4.167E8	59.0
Q5L7N5	Phosphoenolpyruvate carboxykinase (ATP) OS	Bacteroides fragilis	420.91	17	1	6	12	2.103E8	59.0
A3CL27	Formate--tetrahydrofolate ligase 1 OS	Streptococcus sanguinis	145.32	20	1	2	3	3.296E7	59.0
A6LFQ4	Phosphoenolpyruvate carboxykinase (ATP) OS	Parabacteroides distasonis	438.19	17	5	11	14	2.336E8	58.9
C4ZAW6	Dihydroxy-acid dehydratase OS	Agathobacter rectalis	193.87	6	5	6	6	2.765E7	58.9
B9E299	Dihydroxy-acid dehydratase OS	Clostridium kluyveri	85.82	2	1	2	3	7.244E7	58.8
O09460	Phosphoenolpyruvate carboxykinase (ATP) OS	Anaerobiospirillum succiniciproducens	214.42	21	2	5	5	3.702E8	58.6
B2TIR2	Dihydroxy-acid dehydratase OS	Clostridium botulinum	46.21	2	1	1	1	3.131E6	58.5
B3DTV2	ATP synthase subunit alpha OS	Bifidobacterium longum	383.31	393	9	11	12	5.746E7	58.4
B3DRY6	Bifunctional purine biosynthesis protein PurH OS	Bifidobacterium longum	204.27	2	3	3	3	1.243E8	58.4
A6LIG0	60 kDa chaperonin OS	Parabacteroides distasonis	325.96	2	1	7	10	4.117E8	58.3

medRxiv preprint doi: https://doi.org/10.1101/2021.07.13.21260404; this version posted January 21, 2022. The copyright holder for this preprint (which was not certified by peer review) is the author/funder, who has granted medRxiv a license to display the preprint in perpetuity.
All rights reserved. No reuse allowed without permission.

A5N857	Ribonuclease Y OS	Clostridium kluyveri	85.68	95	1	3	3	4.874E7	58.3
Q8G3N6	Inosine-5'-monophosphate dehydrogenase OS	Bifidobacterium longum	685.57	20	15	16	19	2.005E8	58.2
Q8A6P8	60 kDa chaperonin OS	Bacteroides thetaiotaomicron	591.81	1	2	11	15	2.794E8	58.2
Q5LAF6	60 kDa chaperonin OS	Bacteroides fragilis	690.75	1	4	15	20	5.301E8	58.2
A0Q2T1	60 kDa chaperonin OS	Clostridium novyi	58.42	6	2	2	2	2.212E8	58.1
A6KXA0	60 kDa chaperonin OS	Bacteroides vulgatus	948.24	1	11	22	26	6.146E8	58.1

Note: *Score:* The Mascot score. Proteins: The total number of proteins contained in the protein group. *Unique Peptides:* The total number of peptides unique to the protein group. *Peptides:* The total number of peptides identified from all included searches for the master protein of the protein group. *PSMs:* The total number of peptide-spectrum matches identified from all included searches for the master protein of the protein group. *Area:* The chromatographic peak area was used to characterize the quantitative abundance of protein.*MW(kDa):* The theoretical molecular weight of the protein.

medRxiv preprint doi: https://doi.org/10.1101/2021.07.13.21260404; this version posted January 21, 2022. The copyright holder for this preprint (which was not certified by peer review) is the author/funder, who has granted medRxiv a license to display the preprint in perpetuity. All rights reserved. No reuse allowed without permission.